Running head:

**DOWNSYSTEM GRAIN-SIZE TRENDS OF ANCIENT WAVE-INFLUENCED SEDIMENT ROUTING SYSTEM**

Title:

# DOWNSYSTEM GRAIN-SIZE TRENDS AND MASS BALANCE OF AN ANCIENT WAVE-INFLUENCED SEDIMENT ROUTING SYSTEM: MIDDLE JURASSIC BRENT DELTA, NORTHERN NORTH SEA, OFFSHORE UK AND NORWAY

Author:

IKENNA C. OKWARA[1,2], GARY J. HAMPSON*[1], ALEXANDER C. WHITTAKER[1] & GARETH G. ROBERTS[1]

[1]Department of Earth Science and Engineering, Imperial College London, South Kensington Campus, London SW7 2AZ, U.K.

[2] Department of Geology, University of Nigeria, Nsukka, Nigeria

*Corresponding author email address: g.j.hampson@imperial.ac.uk

**Abstract**

We reconstruct spatial variations in grain size in the sediment routing system of the data-rich Middle Jurassic Brent Group of the northern North Sea, using published stratigraphic, thickness, palaeogeographic, provenance and age constraints combined with representative core and wireline-log data. Facies associations provide a textural proxy for gravel, sand and mud grain-size fractions, and their distributions define spatio-temporal variations in grain size within four stratigraphic intervals (J22, J24, J26, J32 genetic sequences). Sediment was sourced from the west (Shetland Platform), east (Norwegian Landmass) and south (Mid-North Sea High). The associated sediment routing systems were geographically distinct in the oldest (J22) and youngest (J32) genetic sequences, but combined to feed a large wave-dominated delta ('Brent Delta') in genetic sequences J24 and J26.

Few of the Brent Group sediment routing systems exhibit the downsystem-fining grain-size trend predicted by sediment mass balance theory. Deviations from this reference trend reflect: (1) sparse sampling of channelised fluvial and fluvio-tidal sandbodies in upsystem locations; (2) preferential trapping of sand in underfilled antecedent and syn-depositional, half-graben depocentres in genetic sequences J22 and J32; and (3) nearshore retention of sand by shoaling waves in wave-dominated shoreface and barrier-strandplain systems. This third type of deviation reveals that spatial facies partitioning due to shallow-marine process regime distorts the simple downsystem-fining reference trend, and supports the interpretation that large volumes of predominantly muddy

sediment were bypassed beyond the 'Brent Delta' into neighbouring basins. Our analysis demonstrates a practical approach to interpret sediment supply and sediment dispersal in the stratigraphic record.
**[end of abstract]**

**Keywords:** sediment grain size, sediment mass-balance; sediment routing system; source-to-sink; Brent Group

## 1. Introduction

Sediment supply and accommodation space are widely considered to be the two principal controls on stratigraphic architecture (e.g. Posamentier and Vail, 1988; Catuneanu et al., 2009; Allen et al., 2013; Romans et al., 2016). For instance, coupled landscape-basin models (e.g. Armitage et al., 2011) clearly show how changing sediment supply as opposed to changing accommodation-space generation should give rise to distinct stratigraphic signatures. Sediment supply is often more difficult to constrain than accommodation space, with the result that sediment supply is rarely explicitly interpreted in studies of stratigraphic architecture (e.g. Heller et al., 1993; Galloway, 2001; Brommer et al., 2009; Hampson, 2016; Burgess and Steel, 2017; Zhang et al., 2019). In contrast, source-to-sink studies have developed several approaches over the last two decades to estimate sediment flux from geologic and geomorphic evidence. These include, for instance, the empirical BQART model of suspended sediment load applied to modern or palaeo-catchments (Syvitski and Milliman, 2007; Zhang et al., 2018; Watkins et al., 2019; Lyster et al., 2020; Ravidà et al., 2021), empirical geomorphological scaling relationships (Sømme et al., 2009; Nyberg et al., 2018; Snedden et al., 2018), and palaeohydrological scaling models applied to stratigraphic observations (Holbrook and Wanas, 2014; Bhattacharya et al., 2016; Garefalakis and Schlunegger, 2018). These approaches to estimating sediment flux have been argued to show broad consistency with each other, and with mapped sediment volumes and ages in rich datasets from the stratigraphic record (Brewer at al., 2020; Lyster et al., 2020; Heins, 2023). However, facies-based grain-size data are rarely incorporated into these approaches (e.g. Reynolds, 2019).

Sediment routing systems record the cascade of sediment from its generation by erosion in source regions to deposition in sinks, via a region of sediment transfer (e.g. Allen, 2017). Preferential deposition of coarser grains during sediment transport gives rise to downsystem-fining grain-size trends that can provide a reference for comparison between sediment routing systems when normalised with respect to accommodation space (i.e. 'sediment mass balance '; Fig. 1; Strong et al., 2005; Whittaker et al., 2011; Paola and Martin, 2012; Michael et al., 2013, 2014; Hampson et al., 2014). Thus, downsystem-fining trends in grain size can in principle be used in combination with sediment flux estimates and, potentially, provenance constraints to infer spatio-temporal variations in sediment supply. The extent to which facies partitioning may complicate spatial interpretations of grain size trends remains contentious (c.f. Michael et al., 2013, 2014), but its use offers the means to apply facies-

based sequence stratigraphic analysis to constrain the role of sediment supply on stratigraphic architecture and sediment routing and dispersal (Fig. 1).

In this paper, we reconstruct downsystem variations in grain size within a sediment mass balance context for the well-constrained, data-rich sediment routing systems of the Middle Jurassic Brent Group and coeval strata, northern North Sea, offshore UK and Norway. These strata include some of the most prolific hydrocarbon reservoirs in the North Sea basin (e.g. Husmo et al., 2003), which are now being evaluated for geological $CO_2$ sequestration (e.g. North Sea Transition Authority, 2023). There is an enormous amount of legacy seismic, well, core, and biostratigraphic data and previous work on the Brent Group reservoirs and play in the public domain. In a recent synthesis, Okwara et al. (2023) used these data to estimate the net-depositional sediment mass of the 'Brent Delta' sediment routing system(s) to be 18.9 x $10^6$ Mt (median P50 value, with a range from $10^{th}$ to $90^{th}$ percentile probability values, P10-P90 range, of 14.8 x $10^6$ Mt to 23 x $10^6$ Mt) deposited in 8.1 Myr, resulting in a net-depositional sediment budget of 2.33 Mt/yr (P50 value, with a P10-P90 range of 1.96-2.78 Mt/yr). Okwara et al. (2023) also used the BQART sediment load model of Syvitski and Milliman (2007) with inputs derived from published data to estimate the source-area sediment budget of 17.4 Mt/yr (P50 value, with a P10-P90 range of 13.9-23.0 Mt/yr). Thus the estimated source-area sediment budget is almost an order of magnitude greater than the estimated net-depositional sediment budget. This discrepancy implies that the 'Brent Delta' sediment routing system(s) was oversupplied with sediment, and sediment bypass beyond the 'Brent Delta' is required to achieve sediment mass balance (Okwara et al., 2023). We extend the sediment mass balance analysis of Okwara et al. (2023) by reconstructing grain-size trends within their estimated net-depositional sediment mass.

We aim to constrain and assess sediment supply and dispersal within the wave-dominated 'Brent Delta' using downsystem variations in grain size, and thereby to evaluate potential sediment bypass to more basinward locations. This aim is important because it addresses the extent to which downsystem variations in grain size together with sediment mass balance can provide a simple, pragmatic tool to interpret the role of sediment supply on stratigraphic architecture. The specific objectives of the paper are threefold: (1) to document upsystem-to-downsystem variations in grain size in the Middle Jurassic Brent Group and coeval strata in the northern North Sea; (2) to use these grain-size variations to constrain sediment supply to, dispersal in, and bypass beyond the 'Brent Delta' sediment routing systems; and (3) to compare these results to estimates of sediment supply derived from the BQART sediment-load model (Okwara et al., 2023) and to qualitative constraints from facies models and sequence stratigraphic interpretations of the 'Brent Delta' (e.g. Budding and Inglin, 1981; Scott, 1992; Johannessen et al., 1995; Olsen and Steel, 1995; Løseth and Ryseth, 2003; Went et al., 2013).

## 2. Geological setting

### 2.1. Tectono-stratigraphic and climatic context

The Middle Jurassic Brent Group and associated strata were deposited in the northern part of the North Sea, within a north-south-trending depocentre that subsequently developed into the Viking Graben and Horda Platform (Fig. 2A, B; e.g. Husmo et al., 2003). The proto-Viking Graben depocentre is bounded by the Shetland Platform to the west, Norwegian Landmass to the east, and Mid-North Sea High to the south (Fig. 2B).

The proto-Viking Graben was initiated during Late Permian to Early Triassic rifting (Barton and Wood, 1984; Steel and Ryseth, 1990; Færseth, 1996; Zanella and Coward, 2003; Duffy et al., 2015), and underwent post-rift thermal subsidence during Late Triassic to Middle Jurassic times (Partington et al., 1993; Rattey and Hayward, 1993; Steel, 1993) (Fig. 2C). Middle Jurassic thermal doming and uplift of the Mid-North Sea, south of the proto-Viking Graben, resulted in erosion of Triassic to Lower Jurassic strata here, and the development of an intra-Aalenian unconformity, widely referred to as the 'mid-Cimmerian Unconformity' (Fig. 2B, C; Ziegler, 1990; Underhill and Partington, 1993, 1994). Middle to Late Jurassic strata onlap this unconformity, recording later collapse of the dome (Underhill and Partington, 1993, 1994; Husmo et al., 2003). Subsequent Late Jurassic to Early Cretaceous rifting resulted in development of the trilete North Sea rift, and established the present-day configuration of structural elements, including the Viking Graben and Horda Platform (e.g. Underhill and Partington, 1993; Zanella and Coward, 2003). In the developing Viking Graben, Late Jurassic to Early Cretaceous rifting reactivated some north-south-trending, Permo-Triassic rift faults and generated additional northeast-southwest-trending faults (Færseth, 1996; Zanella and Coward, 2003; Duffy et al., 2015; Phillips et al., 2019).

The proto-Viking Graben depocentre occupied a palaeo-latitude of c. 44-48°N during the Middle Jurassic (Fig. 2A; Ziegler, 1990; Torsvik et al., 2002). Coal petrology, palynological data, palaeo-latitude reconstructions, strontium isotope data, oxygen isotope data, and ocean-atmosphere numerical models indicate that the depocentre was subject to a sub-tropical and humid climate throughout the Middle Jurassic, with mean annual temperature estimated to have been ca. 20°C (Abbink et al., 2001; Sellwood and Valdes, 2006, 2008; Prokoph et al., 2008).

### 2.2. Stratigraphic and palaeogeographic framework of the 'Brent Delta'

The stratigraphic and palaeogeographic framework of the Brent Group and related strata have been documented in many regional, basin-scale studies (e.g. Graue et al., 1987; Helland-Hansen et al., 1992; Mitchener et al., 1992; Johannessen et al., 1995; Sneider et al., 1995; Fjellanger et al., 1996; Hampson et al., 2004). These studies extended previous sedimentological facies analysis and models (e.g. Budding and Inglin, 1981; Richards and Brown, 1986; Livera, 1989; Ryseth, 1989; Livera and Caline, 1990; Scott, 1992; Muto and Steel, 1997; Løseth and Ryseth, 2003; Morris et al., 2003) to develop sequence stratigraphic interpretations calibrated to biostratigraphic data (e.g.

Whitaker et al., 1992; Partington et al., 1993). Palaeogeographies were reconstructed for specific sequence stratigraphic intervals. The resulting sedimentological, stratigraphic and palaeogeographic frameworks are broadly consistent with each other.

In this study, we use the facies-association classification scheme (Table 1) and stratigraphic framework (Fig. 3) synthesised by Okwara et al. (2023), which is based on the "J sequences" (J22, J24, J26, J32) proposed by Mitchener et al. (1992) and applied to a dataset of wells used in previous stratigraphic studies (Fig. 4, Table S1; Mitchener et al., 1992; Sneider et al., 1995; Fjellanger et al., 1996; Hampson et al., 2004; Kieft et al., 2011). Facies associations are based on sedimentological characteristics in core, and are calibrated to wireline-log characteristics in uncored wells and intervals (Table 1). The basic, and widely used, facies model of the Brent Group is of a wave-dominated delta, in which a wave-dominated shoreface and barrier bars were developed in front of a coal-bearing coastal plain containing lagoons and fluvio-estuarine channels (Budding and Inglin, 1981). Weakly wave-influenced (bioturbated) shorefaces and fan deltas were developed locally in the J22 and J32 genetic sequences (e.g. Graue et al., 1987; Helland-Hansen et al., 1992; Johannessen et al., 1995; Fjellanger et al., 1996; Muto and Steel, 1997; Morris et al., 2003; Hampson et al., 2004). Each "J sequence" is a genetic sequence (*sensu* Galloway, 1989) bounded by biostratigraphically calibrated maximum flooding surfaces of basin-wide extent (Partington et al., 1993). Each genetic sequence is outlined below, and illustrated via isopach and palaeogeographic maps (Figs. 5-8), core and wireline logs from representative wells (Fig. S1), and well correlation panels (Fig. S2). We use the revised biostratigraphic picks of Kieft et al. (2011) to refine local definition of the genetic sequences in Norwegian quadrant 15; in particular, these data place the J32 genetic sequence within the coastal-plain and lagoonal deposits of the Sleipner Formation (e.g. well 15/3-3 in Fig. S2C).

The J22 genetic sequence is characterised by regression and subsequent transgression of fluvio-estuarine channels (facies association 2.2, Table 1) and weakly wave-influenced (bioturbated) shorefaces (facies association 3.1, Table 1), comprising the Broom Formation, from the western basin margin (Figs. 5B, S1A, C, S2A; e.g. Mitchener et al., 1992; Hampson et al., 2004). At the same time, fluvio-estuarine channels and fan deltas (facies association 2.2, Table 1), comprising the Oseberg Formation, underwent regression and subsequent transgression from the eastern basin margin (Figs. 5B, S1B, S2B; e.g. Mitchener et al., 1992; Sneider et al., 1995; Fjellanger et al., 1996). Coeval coastal plain strata (facies associations 1.1-1.3, Table 1), including the Bruce 'C' Sands, accumulated during minor northward shoreline regression and subsequent transgression in the southernmost basin axis (Figs. 5B, S2C; e.g. Mitchener et al., 1992). Thickness changes in the J22 genetic sequence (Fig. 5A) are relatively small. They are either confined to the hangingwalls of a few extensional faults or occur above deeply buried, fault-bounded depocentres developed during Lower Triassic rifting (Fig. 2C). The former are aligned sub-parallel to palaeoshoreline trends

(Fig. 5B), suggesting that the hangingwall depocentres of these extensional faults were underfilled prior to, and thus influenced deposition of, the J22 genetic sequence (e.g. Mitchener et al., 1992; Hampson et al., 2004).

The J24 genetic sequence is characterised by northward regression along the basin axis of a wave-dominated shoreface and barrier bar (facies associations 3.2-3.4, Table 1; Rannoch and Etive formations) and associated coastal plain, lagoon and fluvio-estuarine channels (facies associations 1.1-1.3 and 2.1-2.3, Table 1; lower Ness Formation) (Figs. 6B, S1, S2; e.g. Mitchener et al., 1992; Sneider et al., 1995; Fjellanger et al., 1996; Husmo et al., 2003; Hampson et al., 2004). In the J24 genetic sequence (Fig. 6A), thickness changes are confined to the hangingwalls of a few extensional faults and to locations above deeply buried Lower Triassic depocentres (e.g. Folkestad et al., 2014). Palaeoshorelines were oriented approximately west-east (Figs. 6B). Their orientation is nearly perpendicular to, and continues across, syn-depositional extensional faults (Fig. 6B), suggesting that the associated depocentres were filled and/or overfilled (e.g. Hampson et al., 2004). The J24 genetic sequence thins northward of the maximum-regressive palaeoshoreline position (Fig. 6), reflecting underfilling of relatively deep bathymetry offshore of this palaeoshoreline.

The J26 genetic sequence is characterised by continued, minor northward regression followed by aggradation and subsequent transgression of wave-dominated shorefaces and barrier bars (facies associations 3.2-3.4, Table 1; Etive and, locally, Tarbert formations) in the northern part of the basin, and aggradation of coastal plains, lagoons and fluvio-estuarine channels (facies associations 1.1-1.3 and 2.1-2.3, Table 1; upper Ness Formation, Bruce 'B' Sands) further south (Figs. 7B, S1, S2; e.g. Mitchener et al., 1992; Sneider et al., 1995; Fjellanger et al., 1996; Husmo et al., 2003; Hampson et al., 2004). The thickness of the J26 genetic sequence (Fig. 7A) indicates that the few active fault-bounded depocentres were filled and/or overfilled (e.g. Hampson et al., 2004), and that relatively deep, underfilled bathymetry lay offshore of the west-east oriented, maximum-regressive palaeoshoreline position (Fig. 7).

The J32 genetic sequence records the initiation of Upper Jurassic rifting (Figs. 2C, 3), which is expressed as pronounced thickening into the hangingwalls of extensional faults as they propagated and linked (Fig. S2A; e.g. Davies et al., 2000; McLeod et al., 2000), significant time gaps across unconformities confined to footwall crests and rift shoulders, onlap on to rift-generated topography, and the extrusion of volcanic rocks on the Mid-North Sea High (e.g. Mitchener et al., 1992; Quirie et al., 2019). The genetic sequence is characterised by net-transgressive stacking of a range of shallow- and marginal-marine deposits, including fluvio-estuarine channels and fan deltas (facies association 2.2, Table 1), weakly wave-influenced (bioturbated) shorefaces (facies association 3.1, Table 1), wave-dominated shorefaces (facies associations 3.2-3.4, Table 1) (Tarbert Formation, Bruce 'A' Sands and Hugin Formation) and offshore mudstones (facies association 3.4, Table 1; Heather Formation), which overlie aggradational coastal-plain and lagoonal deposits (facies associations 1.1-1.3 and 2.1-2.3, Table 1; upper Ness

Formation and Sleipner Formation) (Figs. 8B, S1, S2; e.g. Mitchener et al., 1992; Sneider et al., 1995; Fjellanger et al., 1996; Husmo et al., 2003; Hampson et al., 2004). Palaeoshorelines near the base of the J32 genetic sequence were oriented west-east (cf. Fig. 7B), but evolved to a north-south orientation, parallel to major fault trends in the basin and consistent with the development of underfilled hangingwall depocentres, as they retreated towards the basin margins (Fig. 8B).

**2.3. Provenance and sediment source areas**

Petrographic data (e.g. Morton, 1985, 1992; Hamilton et al., 1987; Hurst and Morton, 1988; Mearns, 1992) and palaeogeographic reconstructions (e.g. Mitchener et al., 1992; Fjellanger et al., 1996; Husmo et al., 2003) indicate that sediment was routed consistently to the 'Brent Delta' from three main source areas at the margins of the proto-Viking Graben: the Shetland Platform, Norwegian Landmass, and Mid-North Sea High (Fig. 2B; e.g. Okwara et al., 2023). The Norwegian Landmass lay to the east (Fig. 2B), was composed of Precambrian gneisses and granites and Caledonian metasediments and granitic rocks (Husmo et al., 2003; Morton et al., 2004), and had an estimated relief of 1-1.2 km during the Middle Jurassic (Gabrielsen et al., 2010; Medvedev and Hartz, 2015; Okwara et al., 2023). The Shetland Platform lay to the west (Fig. 2B), and was composed mainly of Devonian, Carboniferous and Permo-Triassic sedimentary rocks reworked from Precambrian metasediments of greenschist to upper amphibolite grade, Caledonian granites, and quartzofeldspathic gneisses (Zanella and Coward, 2003; Morton et al., 2004). The palaeotopography of Shetland Platform catchments is poorly constrained (e.g. Okwara et al., 2023 used a value of 1.0 km in their application of the BQART sediment load model, assuming a similar uplift history to the Norwegian Landmass). The Mid-North Sea High lay to the south (Fig. 2B), was composed of sandstone-dominated Triassic and mudstone-dominated Lower Jurassic sedimentary rocks eroded at the 'mid-Cimmerian Unconformity' (Fig. 2B, C; Ziegler, 1990; Underhill and Partington, 1993, 1994), and had a maximum relief of 0.3-0.5 km (Underhill and Partington, 1993; Okwara et al., 2023).

**2.4. Source-area and depositional-sink sediment budgets**

Okwara et al. (2023) used a synthesis of previous work on the sedimentology, stratigraphy, provenance and source areas of the 'Brent Delta' sediment routing system(s) to estimate the sediment mass supplied from the source areas, the mass of sediment deposited in the deltaic strata, and related sediment budgets. The source-area sediment budget was estimated using the BQART sediment load model of Syvitski and Milliman (2007) and independent geometrical reconstruction of eroded volumes from the Mid-North Sea High source area. The sediment mass in the 'Brent Delta' depositional sink was reconstructed using isopach maps, palaeogeographic reconstructions and facies analysis of core and well-log data, and its mean net-depositional sediment budget was estimated as 2.0-2.8 Mt/yr. In detail, the net-depositional sediment budget increased from 0.24-0.69 Mt/yr for the J22 genetic sequence to 2.54-8.09 Mt/yr for the J32 genetic sequence. Okwara et al. (2023) attributed this increase to thermal doming and uplift of

the Mid-North Sea High source area (cf. Underhill and Partington, 1993, 1994), uplift of the Norwegian Landmass source area (cf. Gabrielsen et al., 2010; Ksienzyk et al., 2014; Medvedev and Hartz, 2015), and potential catchment area expansion, and rift-related uplift of the Shetland Platform and Norwegian Landmass during deposition of the J32 genetic sequence (cf. Helland-Hansen et al., 1992; Davies et al., 2000; Folkestad et al., 2014). The total sediment budget supplied by the three source areas was estimated as 13.9-23 Mt/yr, an order of magnitude higher than the net-depositional sediment budget, which implies significant bypass of sediment beyond the mapped limits of the 'Brent Delta' depocentre (Okwara et al., 2023).

## 3. Dataset and method

### 3.1. Dataset

We use data from 84 representative exploration wells (Fig. 4, Table S1), each of which has been interpreted in previous studies within one of four regional genetic stratigraphic and sequence stratigraphic frameworks (Mitchener et al., 1992; Sneider et al., 1995; Fjellanger et al., 1996; Hampson et al., 2004; Fig. 3). Wells were selected based on their geographical distribution (Fig. 4B) and their use in existing regional genetic stratigraphic and sequence stratigraphic frameworks (Mitchener et al., 1992; Sneider et al., 1995; Fjellanger et al., 1996; Hampson et al., 2004; Fig. 3, Table S1). These regional frameworks are all based on lithofacies interpretations that are consistent with each other and that capture the full range of facies associations in the 'Brent Delta' sediment routing system(s), as summarised in Table 1 (after Supplementary Material of Okwara et al., 2023). In parts of the study area that contain many closely spaced fields with Brent Group reservoirs (e.g. the southern part of UK quadrant 211 and northern part of UK quadrant 3; Fig. 4B), we were able to select wells from a large number of candidates. Other parts of the study area contain only few wells that penetrate Middle Jurassic strata (e.g. UK quadrant 9 and Norwegian quadrants 24 and 25; Fig. 4B). 1360 m of core from eight of the 84 studied wells (Table S2) was described using sedimentological facies analysis, in order to define the overall lithological and grain-size characteristics of facies associations, and to calibrate the lithological composition of uncored intervals and wells (see Supplementary Material of Okwara et al., 2023 for details). The isopach and palaeogeographic maps of Okwara et al. (2023) were used to constrain the thickness and gross facies-association distributions of the J22, J24, J26 and J32 genetic sequences between the studied wells (Figs. 5-8).

### 3.2. Method

In our analysis, we first use steps i-iii of the method of Okwara et al. (2023) to estimate the net-depositional sediment mass of the 'Brent Delta' deposits: (1) definition of age-constrained stratigraphic intervals (J22, J24, J26 and J32 genetic sequences in Fig. 3); (2) facies analysis to constrain the distribution of coastal-plain, marginal-

marine, and shallow-marine-to-shelf deposits in each stratigraphic interval (Table 1); and (3) generation of isopach maps for each stratigraphic interval (Figs. 5A, 6A, 7A, 8A).

The fourth step in our method is delineation of sediment routing system(s) in each stratigraphic interval using palaeogeographic maps (Figs. 5B, 6B, 7B, 8B). In the J22 and J32 genetic sequences, palaeoshorelines adjacent to the western, eastern and southern basin margins are palaeogeographically distinct (Figs. 5B, 8B), such that we consider each of them to belong to a separate sediment routing system (or a combined group of closely spaced sediment routing systems) lying directly downsystem of, and fed by, each source area. In the J24 and J26 genetic sequences, these three sediment routing systems are considered to combine, such that they fed a single west-east-trending palaeoshoreline (Figs. 6B, 7B). For these genetic sequences, we can only analyse the combined sediment routing system. The resulting delineation of sediment routing system(s) is consistent with that of Okwara et al. (2023, their figure 12), which was based on the detrital garnet compositional data of Morton (1992). However, a smaller proportion of the J22 and J32 deposits is sampled (i.e. cumulative area of three red boxes in Figs. 5, 8) than of the J24 and J26 deposits (i.e. area of one red box in Figs. 6, 7), due to the absence of clear palaeogeographic boundaries between sediment routing systems in the J22 and J32 genetic sequences.

The fifth step is calculation in each sediment routing system in each stratigraphic interval of: sediment volumes; volumetric proportions of facies associations; volumetric proportions of broad grain-size classes (gravel, sand, mud); and proportions of the broad grain-size classes by sediment mass. Our fifth step is equivalent to step iv in the method of Okwara et al. (2023), but is applied to the sediment routing systems in each stratigraphic interval, as identified in our fourth step, rather than to the entire stratigraphic interval. This fifth step requires the assumption that each facies association has a constant grain-size composition that is independent of upsystem-to-downsystem position (cf. Hampson et al., 2014). This assumption is consistent with previous facies analyses of the 'Brent Delta' deposits (Table 1; see Supplementary Material of Okwara et al., 2023 for details), which we consider to reflect deposition on a broad, low-gradient coastal plain and shelf that was subject to little direct influence from upstream variations in water discharge and sediment transport capacity. The assumption also does not account for grain-size variations within the proportions of gravel, sand and mud in each facies association. Use of the assumption allows variations in the proportion of facies associations from upsystem to downsystem to be treated as a first-order descriptor of trends in grain size at the scale of the sediment routing system (i.e. "architectural fining" of Hampson et al., 2014), but is not appropriate to analyse more subtle grain-size variations .

To implement the fifth step in our method, the following proximal-to-distal transects were constructed for each sediment routing system in the J22 and J32 genetic sequences: (1) west to east transect for systems fed from the Shetland Platform (Figs. 5, 8); (2) east to west transect for systems fed from the Norwegian Landmass (Figs. 5, 8);

and (3) south to north transect for systems fed from the Mid-North Sea High (Figs. 5, 8) or, in the J24 and J26 genetic sequences, the combination of all three sediment source areas (Figs. 6, 7). Wells and groups of 2-14 wells that are closely spaced (<2 km) along depositional strike (i.e. perpendicular to the proximal-to-distal transect) were projected into the transect lines (in red boxes in Figs. 5-8). The proportions of each facies association were calculated in each projected well, using wireline-log data calibrated to cores (e.g. Figs. S1, S2), and mean facies-association proportions were calculated in each projected group of closely spaced wells. The proportions of gravel, sand and mud grain size classes in each projected well and projected group of wells were calculated from these facies-association proportions and the proportions of gravel, sand and mud assigned to each facies association (Table 1). The wells and groups of wells therefore provide estimates of facies-association proportions and grain-size proportions at specific downsystem distances in each sediment routing system transect. Facies-association proportions and associated grain-size proportions at other points in each transect were estimated by simple linear interpolation between neighbouring pairs of wells and groups of wells in the transect. Facies-association and grain-size volumes between wells were estimated by multiplying the along-strike (i.e. transect-perpendicular) volumetric increments between wells by the mean facies-association and grain-size proportions of the pair of wells that bound each volumetric increment. The sum of these along-strike (i.e. transect-perpendicular) facies-association and grain-size volumetric increments for a particular transect constitutes the facies-association and grain-size volumes in the corresponding sediment routing system. Compacted grain-size volumes along each proximal-to-distal transect are converted to sediment masses using bulk-density values derived from density logs in the studied wells. Gravel conglomerates and sandstones are assigned a bulk density of 2400 $kgm^{-3}$, and mudstones a bulk density of 2500 $kgm^{-3}$ (cf. Okwara et al., 2023). These values include the effects of compaction and cementation. Coal, which is generated biogenically *in situ* (e.g. Budding and Inglin, 1981; Livera, 1989), is excluded from our calculations of sediment mass.

The sixth, and final, step in our method is calculation of downsystem extraction of sediment mass in each sediment routing system in each stratigraphic interval, using the proximal-to-distal transects described above in the fifth step (i.e. in the red boxes shown in Figs. 5-8). The resulting downsystem extraction of sediment mass is normalised against the cumulative sediment mass in the sediment routing system volume (i.e., the parameter Chi, $\chi$, of Strong et al. 2005), in order to provide a framework for comparison between the sediment routing systems (Strong et al. 2005; Paola and Martin, 2012). $\chi(x)$ is defined as:

$$\chi(x) = \int_0^x r_{\Delta T}\,(x)\mathrm{d}x \,/\, \int_0^L r_{\Delta T}\,(x)\mathrm{d}x \qquad (1)$$

where $r(x)$ is the rate of deposition (in dimensions $LT^{-1}$) at a given downstream distance $x$, measured over a time interval $\Delta T$, and $L$ is the total length of the depositional system (Strong et al. 2005). For each sediment routing system, the value assigned to $\Delta T$ is the duration of genetic sequence J22, J24, J26 or J32 (Fig. 3), as appropriate, and the value assigned to $L$ is the length of the proximal-to-distal transect for the relevant sediment routing system (Figs. 5-8).

For each of the sediment routing systems, downsystem changes in the fractions of gravel, sand and mud grain-size classes are described in terms of $\chi$ (Equation 1), with the total sediment mass for each sediment routing system defined for deposits in the area enclosing the proximal-to-distal transect of that system (i.e. by the red boxes in Figs. 5-8). We also evaluate downsystem changes in the fraction of sand deposited in coastal-plain, marginal-marine and shallow-marine-to-shelf environments (Table 1), normalized to the sediment mass extracted by deposition (i.e., $\chi$; Equation 1), along each proximal-to-distal transect (Figs. 5-8).

**3.3. Uncertainties**

Okwara et al. (2023) used a Monte Carlo approach to characterise error and uncertainty in their net-depositional sediment budget (their figure 9), and their results are directly relevant to steps 1, 3 and 5 in our method. Uncertainties related to stratigraphy, age models, sediment volume calculations, and sediment volume-to-mass conversion are discussed and quantified in Okwara et al. (2023).

Uncertainty in the facies-association scheme that we use as a proxy for grain-size distributions (step 2) arises from the quantity, quality and representativeness of core data that constrain the definition of facies associations and their constituent grain-size-class proportions (Table 1), and in the calibration of wireline logs with core data to interpret facies associations in uncored wells and intervals (e.g. Figs. S1, S2). Although we use a relatively small length of core (Table S2) and small number of wells (Fig. 4, Table S1) to construct the facies-association scheme, it is similar to that used in many previous sedimentological studies of the Brent Group at local, sub-regional and regional scales (Budding and Inglin, 1981; Richards and Brown, 1986; Graue et al., 1987; Livera, 1989; Ryseth, 1989; Livera and Caline, 1990; Mitchener et al., 1992; Scott, 1992; Johannessen et al., 1995; Fjellanger et al., 1996; Muto and Steel, 1997; Løseth and Ryseth, 2003; Morris et al., 2003; Hampson et al., 2004). We also use a simple grain-size characterisation scheme with only three major grain-size classes (gravel, sand, mud), which helps to promote standardisation between different sedimentological studies (cf. "grain size bookkeeping" of Reynolds, 2019) and thereby mitigate some uncertainty.

Delineation of the sediment routing system(s) in each stratigraphic interval (step 4) depends on the type, distribution, and quality of data that underpin reconstructions of palaeogeography (Figs. 5-8; e.g. Mitchener et al.,

1992; Fjellanger et al., 1996; Husmo et al., 2003) and provenance (e.g. Morton, 1985, 1992; Hamilton et al., 1987; Hurst and Morton, 1988; Mearns, 1992). Uncertainty is defined by different palaeogeographic scenarios, and is mitigated in our analysis by using a simple model of three sediment source areas in the J22 and J32 genetic sequences that are amalgamated in the J24 and J26 genetic sequences (Figs. 5-8).

Uncertainty in calculating facies-association and grain-size volumes in sediment routing systems (step 5) reflects the quantity, quality and distribution of well data that underpin characterisation of facies-association volumes in the proximal-to-distal transect for each sediment routing system (e.g. Figs. 5-8, S1, S2). Uncertainty may arise because the wells and groups of wells in each sediment routing system transect are not representative of along-strike facies-association distributions. Uncertainty is greater where facies-associations pinch out laterally along-strike, for example because the facies associations occur in channelised bodies. Such uncertainty is qualitatively assessed in our analysis by comparing the mean facies-association and grain-size proportions for groups of wells projected into the transect with the facies-association and grain-size proportions of individual wells in the group. It could be reduced by incorporating additional well data that constrain the distribution and pinch-out relationships of facies associations, particularly those that have channelised and lenticular geometries, but only at the expense of the time required for analysis. Given the large uncertainties in other steps in our method and absence of wells in large parts of the study area (Fig. 4), we consider that the well database is sufficient for indicative, first-order approximations.

Uncertainty in the calculation of downsystem extraction of sediment mass (step 6) is compounded from sources of uncertainty in steps 1-5 of the methodology. In similar studies of ancient sediment routing systems, such compounded errors can result in halving or doubling of net-depositional mass flux estimates (e.g. Galloway, 2001; Hampson et al., 2014).

### 3.4. Outputs

Within the normalised sediment mass framework that is produced by the method outlined above, and associated uncertainty, we compare two parameters from upsystem to downsystem.

The first parameter is the proportion of gravel, sand, and mud grain-size classes in the sediment volume deposited by the sediment routing system in the proximal-to-distal transect. These grain-size proportions have been previously demonstrated to be independent of spatial variations in $\chi$ (Whittaker et al., 2011; Michael et al., 2013). Consequently, differences in grain-size proportions between sediment routing systems and/or between stratigraphic intervals can be attributed to: (1) the grain-size distribution input to the system; (2) along-strike influx

to or efflux from the system; and/or (3) the grain-size distribution of bypassed sediment output from the system (cf. Hampson et al., 2014).

The first of these three mechanisms incorporates any input of sediment via reworking at regional or sub-regional unconformities (e.g. locally coinciding with the base of the J22 and J32 genetic sequences; Fig. 3), as well as fluvial sediment input from source-area catchments. The impact of sediment reworking, temporary sediment storage and autogenic sedimentation processes is more pronounced over shorter time intervals (i.e. small values of $\Delta T$ in Equation 1; e.g. Strong et al. 2005), and is minimised in our analysis by considering genetic sequences of long duration (0.9-3.9 Myr) that are bounded regionally by maximum flooding surfaces (Fig. 3). The second mechanism suggests that the sediment routing system is not closed, consistent with deposition in a wave-dominated delta(s) or other shorelines with significant along-shore sediment transport by waves, tides and marine currents (e.g. Hampson et al., 2014). The third mechanism would suggest that the full downsystem extent of the system has not been mapped, as has recently been implied for the 'Brent Delta' sediment routing system(s) by the sediment mass balance analysis of Okwara et al. (2023).

The second parameter is the downsystem change in percentage-thickness, as a function of sediment mass extracted, of coastal-plain, marginal-marine, and shallow-marine-to-shelf sandstones. This parameter describes the upsystem-to-downsystem position of the palaeoshoreline, relative to the mass fraction of sandstone, in each sediment routing system, and may thus provide insights into the role of along-shore sand transport by waves, tides and marine currents.

## 4. Results

### 4.1. Grain-size fractions of the total sediment mass

#### *4.1.1. Description*

Similar grain-size fractions occur in the J22, J24, J26 and J32 genetic sequences, with gravel, sand and mud constituting 0.7-2.1%, 45-62% and 38-54% of the total sediment mass, respectively (Fig. 9B). Given the large uncertainty in net-depositional sediment budget (Fig. 11A; Okwara et al., 2023), it appears that the grain-size fractions supplied to the 'Brent Delta' sediment routing system(s) remained approximately uniform throughout its deposition. The mean grain-size fractions of the total sediment mass for the J22, J24, J26 and J32 genetic sequences in combination are 1.0% gravel, 55% sand and 44% mud.

#### *4.1.2. Interpretation*

Given the similarity in the gravel, sand and mud grain-size fractions of the net-depositional sediment mass in the J22, J24, J26 and J32 genetic sequences, combined with the apparent regional consistency in heavy mineral provenance characteristics between these genetic sequences (Mearns, 1992; Morton, 1992), we speculate that sediment of a relatively uniform grain-size composition may have been supplied via sediment routing systems from the Shetland Platform, Norwegian Landmass and Mid North Sea High source areas. However, we lack detailed, quantitative petrographic and geochemical data to rigorously test this speculation (cf. Caracciolo, 2020). The similarity in grain-size fractions of the net-depositional sediment mass in each genetic sequence (Figs. 9B) implies either that: (1) the relative proportions of sediment supplied are insensitive to increases in catchment erosion rates, as required to account for the increase in sediment flux from J22 to J32 (Fig. 9A); or (2) the excess of a particular grain-size fraction is preferentially retained in source-area catchments (e.g. gravel) or bypassed downsystem beyond the depositional limit of the 'Brent Delta' (e.g. mud; Okwara et al., 2023).

### 4.2. Downsystem changes in gravel, sand and mud fractions

#### *4.2.1. Genetic sequence J22*

**4.2.1.1. Description.** In genetic sequence J22, there are clear downsystem decreases in gravel and sand fractions in the deposits of sediment routing systems sourced from the Shetland Platform to the west (Figs. 5, 10A; Table S3) and from the Mid North Sea High to the south (Figs. 5, 10C; Table S3). Deposits of the sediment routing system sourced from the Norwegian Landmass to the east exhibit more variable upsystem-to-downsystem changes in gravel and sand fractions, including localised downsystem increases and downsystem decreases, such that there is no overall trend (Figs. 5, 10B). These latter changes in sand fraction occur within shallow-marine-to-shelf environments, rather than in coastal-plain and marginal-marine environments that contain channelised sandbodies (Fig. 10E).

**4.2.1.2. Interpretation.** Downsystem decreases in gravel and sand fractions in deposits of the sediment routing systems sourced from the Shetland Platform and Mid North Sea High occur at $\chi = 0.5$ and $\chi = 0.6$, respectively (Fig. 10A, C), and are consistent with downsystem-fining due to sediment mass extraction by deposition (e.g. simple eastward pinchout of facies association 2.2, 3.1 and 3.2 sandstones in genetic sequence J22, Fig. S2A) (Strong et al., 2005; Paola and Martin, 2012). The more complex changes in sand fraction in deposits of the sediment routing system sourced from the Norwegian Landmass (Fig. 10B) are attributed to preferential accumulation of sand in fan deltas (facies association 2.2, Table 1) located in antecedent half-graben depocentres (Fig. 5A; Graue et al., 1987; Helland-Hansen et al., 1992; Muto and Steel, 1997). Sediment routing from the Norwegian Landmass to these fan deltas was likely controlled by the three-dimensional topography associated with the antecedent half-graben, and is poorly approximated by the two-dimensional, proximal-to-distal transect used to characterise grain-size

distribution (e.g. complex westward and eastward pinchouts of facies association 2.2 and 3.1 sandstones in genetic sequence J22, Fig. S2B).

### *4.2.2. Genetic sequence J24*

**4.2.2.1. Description.** In genetic sequence J24, downsystem changes in grain-size fractions are considered in the context of a single, composite sediment routing system sourced from the Shetland Platform, Mid North Sea High and Norwegian Landmass (Figs. 6, 11A; Table S4). The deposits of the composite sediment routing system exhibit a downsystem increase in sand fraction (from $\chi = 0$ to $\chi = 0.3$, Fig. 11A), followed by a relatively uniform sand fraction (from $\chi = 0.3$ to $\chi = 0.9$, Fig. 11A) and a rapid downsystem decrease in sand fraction (from $\chi = 0.9$ to $\chi = 1.0$, Fig. 11A). The changes in sand fraction reflect an overall downsystem decrease in the proportion of coastal-plain and marginal-marine sand (from $\chi = 0$ to $\chi = 0.9$, Fig. 11B) and a corresponding overall downsystem increase in the proportion of shallow-marine-to-shelf sand (from $\chi = 0.1$ to $\chi = 0.9$, Fig. 11B), followed by a rapid downsystem decrease in the proportion of shallow-marine-to-shelf sand (from $\chi = 0.9$ to $\chi = 1.0$, Fig. 11B).

**4.2.2.2. Interpretation.** These changes in sand fraction are interpreted to reflect sand accumulation predominantly in coastal-plain and marginal-marine channels in upsystem locations (from $\chi = 0$ to $\chi = 0.3$, Fig. 11; facies association 1.1 and 2.2 sandstones in genetic sequence J24, Fig. S2C), sand accumulation in a northward-prograding, wave-dominated shoreface and barrier-strandplain system (from $\chi = 0.3$ to $\chi = 0.9$, Fig. 11; Fig. S2), and palaeoseaward-decreasing sand content at the northward-progradational limit of the wave-dominated shoreface and barrier-strandplain system (from $\chi = 0.9$ to $\chi = 1.0$, Fig. 11; facies association 3.2 and 3.3 sandstones in genetic sequence J24, Figs. 6B, S2C) (Graue et al., 1987; Helland-Hansen et al., 1992; Mitchener et al., 1992; Fjellanger et al., 1996; Hampson et al., 2004).

### *4.2.3. Genetic sequence J26*

**4.2.3.1. Description.** Downsystem changes in grain-size fractions in genetic sequence J26 are also considered in the context of a single, composite sediment routing system (Figs. 7, 12A; Table S5). The associated deposits exhibit a relatively uniform sand fraction over much of their upsystem-to-downsystem extent (from $\chi = 0$ to $\chi = 0.9$, Fig. 12A), but with two localised maxima (at $\chi = 0.1$ and $\chi = 0.9$, Fig. 12A), followed by a rapid downsystem decrease in sand fraction (from $\chi = 0.9$ to $\chi = 1.0$, Fig. 12A).

**4.2.3.2. Interpretation.** In most upsystem-to-downsystem locations (from $\chi = 0$ to $\chi = 0.9$, Fig. 12B), the sand fraction is interpreted to reflect sampling of coastal-plain and marginal-marine channels (Fig. S2). At downsystem distances for which multiple wells are grouped (e.g. for which $n \geq 4$, Fig. 12), there is sufficient sampling of channels and intervening interfluves that the mean value of sand fraction is constrained between 30 and 60% (Fig. 12). At

downsystem distances for which only one well is present (i.e. for which n = 1, Fig. 12), unrepresentatively high or low values of sand fraction are recorded (e.g. 90% in the localised peak at $\chi = 0.1$, Fig. 12) depending on whether a channel or interfluve is sampled. The rapid downsystem decrease in sand fraction in downsystem locations (from $\chi = 0.9$ to $\chi = 1.0$, Fig. 12) is interpreted to reflect palaeoseaward-decreasing sand content at the northward-progradational limit of the wave-dominated shoreface and barrier-strandplain system (facies association 3.2 and 3.3 sandstones in genetic sequence J26, Figs. 7B, S2C; Graue et al., 1987; Helland-Hansen et al., 1992; Mitchener et al., 1992; Fjellanger et al., 1996; Hampson et al., 2004).

#### *4.2.4. Genetic sequence J32*

**4.2.4.1. Description.** Three distinct sediment routing systems are identified in genetic sequence J32 (Figs. 8, 13A-C; Table S6). Deposits of the sediment routing system sourced from the Shetland Platform to the west (Fig. 8) exhibits an overall downsystem decrease in sand fraction, but with a localised minimum between $\chi = 0.1$ and $\chi = 0.3$, in its deposits (Fig. 13A). Deposits of the sediment routing systems sourced from the Mid North Sea High to the south and from the Norwegian Landmass to the east (Fig. 8) both lack simple upsystem-to-downsystem trends in gravel and sand fractions (Fig. 13B, C). For example, deposits of the sediment routing system sourced from the Norwegian Landmass High (Fig. 8) exhibit a downsystem increase in sand fraction (from $\chi = 0$ to $\chi = 0.4$, Fig. 13B) followed by an irregular decrease in sand fraction (from $\chi = 0.4$ to $\chi = 1.0$, Fig. 13B). The changes in sand fraction occur within shallow-marine-to-shelf environments, rather than in coastal-plain and marginal-marine environments, which are less abundant in the deposits of this sediment routing system (Fig. 13E). The sand fraction of deposits of the sediment routing system sourced from the Mid North Sea (Fig. 8) increases downsystem overall, but this increase is subtle and masked by shorter-period changes (Fig. 13C). This overall trend is composed of an irregular downstream decrease in the sand fraction within coastal-plain and marginal-marine channels (Fig. 13F), combined with a downstream increase in the sand fraction within shallow-marine-to-shelf environments (from $\chi = 0.3$ to $\chi = 1.0$, Fig. 13F).

**4.2.4.2. Interpretation.** We attribute the upsystem-to-downsystem changes in sand fraction in deposits of the sediment routing systems sourced from the Shetland Platform and Norwegian Landmass (Fig. 13) to the initiation and growth of syn-depositional faults that are interpreted to have generated complex, three-dimensional patterns in sediment routing and accumulation (Fig. 8; Helland-Hansen et al., 1992; Mitchener et al., 1992; Fjellanger et al., 1996; Davies et al., 2000; McLeod et al., 2002; Hampson et al., 2004). These complex, three-dimensional patterns are poorly approximated by the two-dimensional, proximal-to-distal transects that we have used to characterise grain-size distribution (e.g. complex westward and eastward thickness variations and pinchouts of facies association 3.1-3.4 sandstones in genetic sequence J32, Fig. S2A, B). In the deposits of the sediment routing system sourced from the Mid North Sea High, upsystem-to-downsystem changes in the sand fraction are attributed to sparse sampling

of coastal-plain and marginal-marine channels in well data ($n \leq 3$ at all downsystem distances, Fig. 13C, F; facies association 1.1 and 2.2 sandstones in genetic sequence J32, Fig. S2A) combined with sand accumulation in a series of retrogradationally stacked, southward-retreating, wave-dominated and weakly wave-influenced shoreface systems (from $\chi = 0.3$ to $\chi = 1.0$, Fig. 13F; facies association 2.2 and 3.1-3.4 sandstones in genetic sequence J32, Fig. S2A, B).

## 5. Discussion

Paola and Martin (2012) argued that simple models of geomorphic relationships and downsystem grain-size fining in a mass-balance framework can provide a useful reference for interpretation of complex, real-world systems that deviate from the simple reference state. Models of closed sediment routing systems (i.e. with no sediment mass transfer to or from neighbouring systems) indicate that grain size fines downsystem, when normalised by the total sediment mass, due to sediment mass extraction by deposition (Strong et al., 2005; Paola and Martin, 2012). Most of the 'Brent Delta' sediment routing systems do not each exhibit a simple downsystem decrease in the proportion of facies associations of a given grain size (Figs. 10A-C, 11A, 12A, 13A-C), and thus differ from reference models.

### 5.1. Why do the 'Brent Delta' deposits not exhibit a simple downsystem-fining trend in the facies-association proxy for grain size?

Although some of the sediment routing systems that we delineate in the 'Brent Delta' deposits exhibit a relatively simple downsystem-fining trend in the proportion of facies associations of a given grain size (Fig. 10A, C), most show more complex upsystem-to-downsystem patterns in the facies-association proxy for grain size (Figs. 10B, 11A, 12A, 13A-C). We identify three reasons for these complex patterns.

First, locally variable, irregular sand fractions in upsystem locations are attributed to sampling of laterally discontinuous, channelised sandbodies in coastal-plain and marginal-marine environments (facies associations 1.1 and 2.2, Table 1) by sparse, relatively widely spaced wells (from $\chi = 0$ to $\chi = 0.3$ in Fig. 11; from $\chi = 0$ to $\chi = 0.9$ in Fig. 12; from $\chi = 0$ to $\chi = 1.0$ in Fig. 13C, F) (Fig. 14). Such local variations may be mitigated by increasing the number of wells, where sufficient well data are available, and thus sampling more representatively the channelised sandbodies and their intervening interfluves.

Second, locally variable sand fractions in non-channelised, marginal-marine and shallow-marine-to-shelf environments (facies associations 2.2 and 3.1-3.4, Table 1) in genetic sequences J22 and J32 are attributed to infilling of rift-related, underfilled antecedent or syn-depositional topography with a complex spatial distribution (Figs. 5A, 8A; from $\chi = 0$ to $\chi = 1.0$ in Figs. 10B, E, 13A-B, D-E). Sediment routing and accumulation in the three-dimensionally

complex topography is sparsely sampled by the two-dimensional, proximal-to-distal transect lines in Figures 5 and 8, which results in pronounced local minima and maxima in sand fraction. The resulting upsystem-to-downsystem patterns in gravel, sand and mud fractions are consistent with established interpretations of laterally stacked fan deltas (facies association 2.2, Table 1) in antecedent half-graben depocentres in genetic sequence J22 (Fig. 5A; Graue et al., 1987; Helland-Hansen et al., 1992; Muto and Steel, 1997) and of shoreface sandstones (facies associations 3.1-3.3, Table 1) in growing, underfilled half-graben depocentres in genetic sequence J32 (Fig. 8A; Helland-Hansen et al., 1992; Mitchener et al., 1992; Fjellanger et al., 1996; Davies et al., 2000; McLeod et al., 2002; Hampson et al., 2004). Where topographic steering of sediment routing systems is clearly defined (e.g. imaged in high-resolution seismic data) and well distribution allows, such undersampling may be mitigated by orienting transects along the axes of the sediment routing systems.

Third, downsystem-increasing or relatively consistent sand fractions in non-channelised, wave-dominated shallow-marine-to-shelf environments (facies associations 2.2 and 3.2-3.4, Table 1) are attributed to prograding or retrograding shoreface and barrier-strandplain systems that are not restricted to underfilled antecedent or syn-depositional depocentres (from $\chi = 0.3$ to $\chi = 0.9$ in Fig. 11; from $\chi = 0.3$ to $\chi = 1.0$ in Fig. 13C, F) (Fig. 14). The progradational limit of such wave-dominated shoreface and barrier-strandplain systems is marked by an abrupt downsystem decrease in sand fraction (from $\chi = 0.9$ to $\chi = 1.0$ in Fig. 11; from $\chi = 0.9$ to $\chi = 1.0$ in Fig. 12) (Fig. 14). These upsystem-to-downsystem patterns in the facies-association proxy for grain size are consistent with established interpretations of wave-dominated, shoreface and barrier-strandplain deposits in genetic sequences J24, J26 and J32 (Fig. 6A, 7A, 8A; Graue et al., 1987; Helland-Hansen et al., 1992; Mitchener et al., 1992; Fjellanger et al., 1996; Hampson et al., 2004). Such wave-dominated shoreface and barrier-strandplain deposits are associated with nearshore retention of sand by shoaling fairweather waves (i.e. the 'littoral energy fence' of Swift and Thorne, 1991) and significant shoreline-parallel sediment transport, for example in response to oblique wave approach (e.g. Komar, 1976), as noted in previous interpretations of wave-dominated shoreface, strandplain and barrier island deposits in the 'Brent Delta' (Fig. 14; e.g. Mearns, 1992; Morton, 1992; Scott, 1992; Løseth and Ryseth, 2003; Went et al., 2013).

For each of these three reasons, spatial facies partitioning obscures downsystem-fining trends, particularly in the point-based observational data provided by wells. Incorporating additional wells may mitigate these effects to an extent, provided that they sample representatively the underlying facies distributions. However, spatial facies partitioning produced by processes that systematically redistribute sediment (e.g. waves and tides in shoreface-shelf settings) are still likely to distort simple downsystem-fining trends. Accounting for these processes requires mapping potentially complex sediment routing and dispersal patterns, as preserved in stratigraphic architectures, and integrating these patterns across all grain-size fractions. In the 'Brent Delta' sediment routing systems, this

approach would require adding the bypassed sediment mass to those characterised herein (Figs. 10-13). If such careful analysis of sediment routing and grain-size fractionation were carried out, sediment mass balance theory predicts that downstream extraction of sediment in $\chi$ space should recover a simple downsystem-fining trend, as documented in physical experiments (e.g. Strong et al., 2005; Paola and Martin, 2012).

### 5.2. Can downsystem changes in the facies-association proxy for grain-size fractions constrain the budget of reworked or bypassed sediment mass?

Source-area sediment budgets, which describe sediment influx from source-area catchments to the 'Brent Delta', are almost one order-of-magnitude larger than the net-depositional sediment budgets for the 'Brent Delta' sediment routing systems (Okwara et al., 2023). This discrepancy can potentially be accounted for by two mechanisms. First, it may have arisen because a large sediment mass underwent net export (or bypass) from the 'Brent Delta' sediment routing systems northwestward to the Faroe-Shetland Basin and/or northward to the western Møre Basin. Second, erosion and sediment reworking at unconformities (e.g. at the base of the J22 genetic sequence, or between the J26 and J32 genetic sequences; Mitchener et al., 1992; Fjellanger et al., 1996; Hampson et al., 2004; Fig. 3) may have reduced the net-depositional sediment budget. Below we consider the likely grain-size distributions released from the source-area catchments and by erosional reworking at unconformities, how these grain-size distributions of the sediment supply compare to downsystem changes in grain-size fractions in the 'Brent Delta' deposits, and the implications for the volume and grain-size characteristics of sediment that was potentially bypassed to the Faroe-Shetland Basin and/or western Møre Basin.

The proportion of gravel, sand and mud generated in, and exported from, catchments reflect their topography, exposed bedrock lithologies, climate, and sediment residence time (e.g. Palomares and Arribas, 1993; Arribas and Tortosa, 2003; Whittaker et al., 2010; Allen et al., 2015; Caracciolo, 2020; Watkins et al., 2020; Heins, 2023). In the source-area catchments that supplied sediment to the 'Brent Delta', the climate was sub-tropical and humid throughout the Middle Jurassic (Abbink et al., 2001; Sellwood and Valdes, 2006, 2008; Prokoph et al., 2008). Catchments on the Norwegian Landmass were composed of Precambrian gneisses and Caledonian metamorphic and granitic rocks (Morton et al., 2004), which probably generated grain-size distributions with a high proportion of medium-to-very-coarse sand and gravel (Palomares and Arribas, 1993; Allen et al., 2015; Fig. 14). Shetland Platform catchments were composed of Devonian, Carboniferous and Permo-Triassic sedimentary rocks (Morton et al., 2004) that likely generated grain-size distributions with variable proportions of sand and gravel; high proportions of fine-to-coarse sand for reworked sandstones and relatively low proportions of sand for reworked mudstones and limestones (Arribas and Tortosa, 2003; Allen et al., 2015; Fig. 14). Sandstone-dominated Triassic and mudstone-dominated Lower Jurassic sedimentary rocks were eroded from catchments on the Mid North Sea High (Underhill and Partington, 1993; Okwara et al., 2023), and probably generated grain-size distributions with

high and low proportions of fine-to-coarse sand, respectively (Arribas and Tortosa, 2003; Allen et al., 2015; Fig. 14). The grain-size distributions generated by fragmentation and weathering (Palomares and Arribas, 1993; Arribas and Tortosa, 2003; Allen et al., 2015) are modified by the duration and intensity of physical and chemical weathering during transport and storage (e.g. Heins and Kairo, 2007), although the resulting grain sizes retain a log-normal distribution (Allen et al., 2017).

Erosion at the base of fluvio-estuarine channels generated a sub-regional unconformity at the base of the J22 genetic sequence (Mitchener et al., 1992; SB177 of Fjellanger et al., 1996; SB100 of Hampson et al., 2004; Fig. 3). The unconformity is cut into marine mudstones of the Dunlin Group, and the volume of eroded mudstones is less than that of marginal-marine sandstones in the J22 genetic sequence (i.e. <190 $km^3$). This volume corresponds to a reworked-sediment mass of <480 Mt and reworked-sediment flux of <0.12 Mt/yr, less than one-third of the net-depositional sediment flux estimated for the J22 genetic sequence (0.43 Mt/yr; Okwara et al., 2023). The base of the J32 genetic sequence is marked by a sub-regional unconformity on the western margin of the Viking Graben, marked by erosion of up to 40 m (typically c. 20 m) of sandstones and mudstones over an area of approximately 40 $km^2$ (SB1000 of Hampson et al., 2004; Fig. 3). The resulting volume of reworked sediment is c. 0.8 $km^3$ , corresponding to a reworked-sediment mass of c. 2 Mt and reworked-sediment flux of c. 2.2 x $10^{-6}$ Mt/yr; this estimated flux is insignificant compared to the net-depositional sediment fluxes estimated for the J26 and J32 genetic sequences (3.1 Mt/yr and 4.1 Mt/yr, respectively; Okwara et al., 2023). In summary, erosional reworking at unconformities can account for very little of the discrepancy between source-area and net-depositional sediment budgets, and we instead invoke sediment bypass.

The downsystem-increasing or relatively consistent sand fractions in wave-dominated shoreface and barrier-strandplain deposits of genetic sequences J24 and J26 (from $\chi = 0.9$ to $\chi = 1.0$ in Fig. 11; from $\chi = 0.9$ to $\chi = 1.0$ in Fig. 12) support the nearshore retention of sand within the 'littoral energy fence' (Swift and Thorne, 1991) and corresponding preferential offshore transport of mud. Thus, the sedimentological characteristics of the high sand fraction of the net-depositional sediment budgets (45-62% in genetic sequences J22-J32; Fig. 9B) are also consistent with significant mud bypass to the Faroe-Shetland Basin and/or western Møre Basin (Fig. 14). In order to balance the sediment mass supplied from source-area catchments with the net-depositional sediment budgets of the 'Brent Delta' deposits solely by trapping gravel and sand within the 'littoral energy fence', a sediment supply of approximately 0.02 Mt/yr of gravel, 1.3 Mt/yr of sand and 18.7 Mt/yr of mud is required, with 17.7 Mt/yr of this mud being exported to the Faroe-Shetland Basin and/or western Møre Basin (i.e. only 1.0 Mt/yr of mud is accounted for in the net-depositional sediment mass; Fig. 9B). This is an end-member estimate, because net-import of sand to wave-dominated shoreface and barrier-strandplain deposits via shoreline-parallel sediment transport, and/or net-export of mud by the same mechanism, can also contribute to balancing the source-area sediment

budgets with the net-depositional sediment budgets. Estimates of sediment supply from the source areas may also be systematic underestimates, because the BQART model considers only suspended sediment load (see Okwara et al., 2023 for discussion). Notwithstanding the assumptions and uncertainties in our analysis, similarly large proportions of sediment bypass, associated with differential transport of sand and mud fractions, are noted in other source-to-sink studies (e.g. Angoche margin, Heins, 2023).

We consider that a combination of: (1) export of variably sandy sediment from the Shetland Platform, Norwegian Mainland and Mid North Sea High source-area catchments; (2) retention of sand in wave-dominated shoreface and barrier-strandplain deposits by the 'littoral energy fence'; and (3) net-import of sand and/or next-export of mud by wave-generated longshore currents can account for much of the discrepancy between source-area sediment budgets and net-depositional sediment budgets of the 'Brent Delta' sediment routing systems (Fig. 14; Okwara et al., 2023).

**5.3. Implications for analysis of sediment routing systems in the stratigraphic record**

The integration of downsystem variations in grain size (e.g. Reynolds, 2019), or a facies-association proxy for grain-size fractions with sediment flux estimates (e.g. Brewer et al., 2020) provides a means to interpret sediment supply as a control on stratigraphic architecture. Such interpretations are not straightforward, and need to be guided by a conceptual model of the sediment routing system(s) that explicitly accounts for spatial facies partitioning. For example, the facies model of a wave-dominated delta ('Brent Delta') is required to interpret retention of sand in shoreface and barrier-strandplain facies by the 'littoral energy fence' (Swift and Thorne, 1991); this nearshore sand retention significantly modifies the simple downsystem-fining trend identified as a reference by Paola and Martin (2012) (Fig. 14). In addition, this facies model implies alongshore sediment transport that is consistent with heavy mineral provenance data (Morton, 1992). It also implies that the 'Brent Delta' sediment routing system(s) was not closed, and that the mapped sediment volumes do not account for the full sediment budget (cf. Angoche margin, Heins, 2023). Other deviations from the reference of a simple downsystem-fining grain-size trend are attributed to preferential trapping of sand and gravel by antecedent and growing, syn-depositional topography, and to sparse, unrepresentative sampling of channelised sandbodies and their coeval sand-poor interfluves. The former may be mitigated by organising and analysing well data along the axes of the sediment routing systems, where the spatial distribution of well data allows. The latter may be mitigated by increasing the number of wells, where sufficient well data are available.

Despite potential ambiguity in interpretations, we consider that the analysis of downsystem grain-size variations in a sediment mass balance context provides insights that constrain sediment supply as a control on stratigraphic architecture. In the context of the 'Brent Delta' sediment routing system(s), downsystem grain-size variations

support the interpretation that large volumes of predominantly muddy sediment were bypassed beyond the down-dip limit of the wave-dominated delta front into the Faroes-Shetland Basin and Møre Basin (Figs. 2, 14). This interpretation is consistent with estimates of sediment supply derived from the BQART sediment-load model (Okwara et al., 2023). In contrast, sequence stratigraphic interpretations are inconsistent, and have proposed either the presence (e.g. Johannessen et al., 1995; Olsen and Steel, 1995) or absence of down-dip sediment bypass from the 'Brent Delta' (e.g. Went et al., 2013).

## 6. Conclusions

We reconstruct upsystem-to-downsystem variations in grain size in the sediment routing systems of the Middle Jurassic (Aalenian – Bathonian) Brent Group and coeval strata of the Northern North Sea in a sediment mass balance framework, in order to constrain sediment supply to the 'Brent Delta'. 'Brent Delta' deposits are subdivided into four previously defined, age-constrained stratigraphic intervals (J22, J24, J26 and J32 genetic sequences), and sediment routing systems delineated in each genetic sequence. Facies associations are used as a textural proxy for gravel, sand and mud grain-size fractions in the net-depositional sediment mass of each sediment routing system. Upsystem-to-downsystem variations in the facies-association proxy for grain-size fractions are normalised with respect to depositional sediment mass, so that they can be readily compared with each other.

A simple downsystem-fining trend in grain size, the reference case predicted by theory and physical experiments, is rare in the 'Brent Delta' sediment routing systems for three reasons. (1) Locally variable, irregular sand fractions in upsystem locations reflect sparse sampling of laterally discontinuous, channelised sandbodies in coastal-plain and marginal-marine environments. (2) Locally variable sand fractions in non-channelised, marginal-marine and shallow-marine-to-shelf environments in transverse sediment routing systems in the J22 and J32 genetic sequences are attributed to preferential trapping of sand in underfilled antecedent and syn-depositional, half-graben depocentres that are poorly represented in simple upsystem-to-downsystem transects. (3) Downsystem-increasing and relatively uniform sand fractions in non-channelised, wave-dominated shallow-marine-to-shelf environments in the J24 and J26 genetic sequences correspond to prograding or retrograding shoreface and barrier-strandplain systems, in which sand was retained near the shoreline by shoaling fairweather waves. By inference, wave-driven alongshore sediment transport was common in the 'Brent Delta' sediment routing system(s), which were not closed systems. This result demonstrates that spatial facies partitioning due to shallow-marine process regime is sufficient to distort the simple downsystem-fining trends predicted by sediment mass balance theory.

The 'Brent Delta' deposits in each genetic sequence have a similar composition by mass: 0.7-2.1% gravel, 45-62% sand and 38-54% mud. These compositions are consistent with net input of sand to and/or net export of mud from

the 'Brent Delta' sediment routing system(s) by alongshore sediment transport. Our reconstructions of upsystem-to-downsystem variations in the facies-association proxy for grain size thus support the interpretation that large volumes of predominantly muddy sediment were bypassed beyond the down-dip limit of the 'Brent Delta', as implied by previous application of the BQART sediment-load model to the Brent Group sediment routing systems.

## Acknowledgements

We thank Robert Duller, two anonymous reviewers, two anonymous Associate Editors and Editor Peter Burgess for their critical reviews and editorial assessments, which greatly improved the manuscript. We also thank Christopher Brewer, Christian Haug Eide, John Holbrook, Christopher Jackson, Howard Johnson and Oliver Jordan for constructive and encouraging discussions of this work, and the British Geological Survey (Nottingham, United Kingdom) and the Norwegian Petroleum Directorate (Stavanger, Norway) for permission to access subsurface core repositories and well data. Our research was supported by the Petroleum Technology Development Fund of Nigeria through a scholarship grant to ICO (project grant number: PTDF/ED/PHD/OIC/848/16).

## References

Abbink, O., Targarona, J., Brinkhuis, H. & Visscher, H. (2001). Late Jurassic to earliest Cretaceous palaeoclimatic evolution of the southern North Sea. Global and Planetary Change, 30, 231-256.

Allen, P.A. (2017). Sediment routing systems: the fate of sediment from source to sink. Cambridge University Press.

Allen, P.A. & Heller, P.L. (2011). Dispersal and preservation of tectonically generated alluvial gravels in sedimentary basins. In C. Busby & A. Azor (Eds.) *Tectonics of sedimentary basins: recent advances* (pp. 111-130). Blackwell.

Allen, P.A., Armitage, J.J., Carter, A., Duller, R.A., Michael, N.A., Sinclair, H.D., Whitchurch, A.L. & Whittaker, A.C. (2013). The Qs problem: sediment volumetric balance of proximal foreland basin systems. Sedimentology, 60, 102-130.

Allen, P.A., Armitage, J.J., Whittaker, A.C., Michael, N.A., Roda-Boluda, D. & D'Arcy, M. (2015). Fragmentation model of the grain size mix of sediment supplied to basins. The Journal of Geology, 123, 405-427.

Allen, P.A., Michael, N.A., D'Arcy, M., Roda-Boluda, D.C., Whittaker, A.C., Duller, R.A. & Armitage, J.J. (2017). Fractionation of grain size in terrestrial sediment routing systems. *Basin Research*, *29*, 180-202.

Armitage, J.J., Duller, R.A., Whittaker, A.C. & Allen, P.A. (2011). Transformation of tectonic and climatic signals from source to sedimentary archive. Nature Geoscience, 4, 231-235.

Arribas, J. & Tortosa, A. (2003). Detrital modes in sedimenticlastic sands from low-order streams in the Iberian Range, Spain: the potential for sand generation by different sedimentary rocks. Sedimentary Geology, 159, 275-303.

Barton, P. & Wood, R. (1984). Tectonic evolution of the North Sea basin: crustal stretching and subsidence. Geophysical Journal International, 79, 987-1022.

Bhattacharya, J.P., Copeland, P., Lawton, T.F. & Holbrook, J. (2016). Estimation of source area, river paleo-discharge, paleoslope, and sediment budgets of linked deep-time depositional systems and implications for hydrocarbon potential. Earth-Science Reviews, 153, 77-110.

Brewer, C.J., Hampson, G.J., Whittaker, A.C., Roberts, G.G. & Watkins, S.E. (2020). Comparison of methods to estimate sediment flux in ancient sediment routing systems. Earth-Science Reviews, 207, 103217.

Brommer, M.B., Weltje, G.J. & Trincardi, F. (2009). Reconstruction of sediment supply from mass accumulation rates in the northern Adriatic Basin (Italy) over the past 19,000 years. Journal of Geophysical Research, 114, 1-15.

Budding, M.C. & Inglin, H.F. (1981). A reservoir geological model of the Brent Sands in southern Cormorant: Petroleum geology of the continental shelf of northwestern Europe. In V. Illing, & G.D. Hobson (Eds.), Petroleum Geology of the continental shelf of north-west Europe (pp. 326-334). Institute of Petroleum.

Burgess, P.M. & Steel, R.J. (2017). How to interpret, understand, and predict stratal geometries using stratal-control spaces and stratal-control-space trajectories. Journal of Sedimentary Research, 87, 325-337.

Caracciolo, L. (2020). Sediment generation and sediment routing systems from a quantitative provenance analysis perspective: review, application and future development. Earth-Science Reviews, 209, 103226.

Catuneanu, O., Abreu, V., Bhattacharya, J.P., Blum, M.D., Dalrymple, R.W., Eriksson, P.G., Fielding, C.R., Fisher, W.L., Galloway, W.E., Gibling, M.R., Giles, K.A., Holbrook, J.M., Jordan, R., Kendall, C.G.St.C., Macurda, B.,

Martinsen, O.J., Miall, A.D., Neal, J.E., Nummedal, D., Pomar, L., Posamentier, H.W., Pratt, B.R., Sarg, J.F., Shanley, K.W., Steel, R.J., Strasser, A., Tucker, M.E. & Winker, C. (2009). Towards the standardization of sequence stratigraphy. Earth-Science Reviews, 92, 1-33.

Davies, S.J., Dawers, N.H., McLeod, A.E. & Underhill, J.R. (2000). The structural and sedimentological evolution of early syn-rift successions: the Middle Jurassic Tarbert Formation, North Sea. Basin Research, 12, 343-365.

Deegan, C.T. & Scull, B.J. (1977). A standard lithostratigraphic nomenclature for the Central and Northern North Sea. Report of the Institute of Geological Sciences, 77/25.

Duffy, O.B., Bell, R.E., Jackson, C.A-L., Gawthorpe, R.L. & Whipp, P.S. (2015). Fault growth and interactions in a multiphase rift fault network: Horda Platform, Norwegian North Sea. Journal of Structural Geology, 80, 99-119.

Færseth, R.B. (1996). Interaction of Permo-Triassic and Jurassic extensional fault-blocks during the development of the northern North Sea. Journal of the Geological Society, 153, 931-944.

Fjellanger, E., Olsen, T.R. & Rubino, J.L. (1996). Sequence stratigraphy and palaeogeography of the Middle Jurassic Brent and Vestland deltaic systems, Northern North Sea. Norsk Geologisk Tidsskrift, 76, 75-106.

Folkestad, A., Odinsen, T., Fossen, H. & Pearce, M.A. (2014). Tectonic influence on the Jurassic sedimentary architecture in the northern North Sea with focus on the Brent Group. In A.W. Martinius, R. Ravnås, J.A. Howell, R.J. Steel & J.P. Wonham (Eds.), From depositional systems to sedimentary successions on the Norwegian Continental Margin. International Association of Sedimentologists, Special Publication 46, 389-416.

Gabrielsen, R.H., Faleide, J.I., Pascal, C., Braathen, A., Nystuen, J.P., Etzelmuller, B. & O'Donnell, S. (2010). Latest Caledonian to Present tectonomorphological development of southern Norway. Marine and Petroleum Geology, 27, 709-723.

Galloway, W.E. (1989). Genetic stratigraphic sequences in basin analysis I: architecture and genesis of flooding-surface bounded depositional units. American Association of Petroleum Geologists Bulletin, 73, 125-142.

Galloway, W.E. (2001). Cenozoic evolution of sediment accumulation in deltaic and shore-zone depositional systems, northern Gulf of Mexico Basin. Marine and Petroleum Geology, 18, 1031-1040.

Garefalakis, P. & Schlunegger, F. (2018). Link between concentrations of sediment flux and deep crustal processes beneath the European Alps. Scientific Reports, 8, 183.

Graue, E., Helland-Hansen, W., Johnsen, J., Lømo, L., Nøttvedt, A., Rønning, K., Ryseth, A. & Steel, R. (1987). Advance and retreat of Brent delta system, Norwegian North Sea. In J. Brooks, & K. Glennie (Eds.) Petroleum Geology of North West Europe, Volume 2 (pp. 915-937). Graham and Trotman.

Hamilton, P.J., Fallick, A.E., Macintyre, R.M. & Elliot, S. (1987). Isotopic tracing of the provenance and diagenesis of Lower Brent Group sands, North Sea. In J. Brooks, & K. Glennie (Eds.) Petroleum Geology of North West Europe, Volume 2 (pp. 939-949). Graham and Trotman.

Hampson, G.J. (2016). Towards a sequence stratigraphic solution set for autogenic processes and allogenic controls: Upper Cretaceous strata, Book Cliffs, Utah, USA. Journal of the Geological Society, 173, 817-836.

Hampson, G.J., Sixsmith, P.J. & Johnson, H.D. (2004). A sedimentological approach to refining reservoir architecture in a mature hydrocarbon province: the Brent Province, UK North Sea. Marine and Petroleum Geology, 21, 457-484.

Hampson, G.J., Duller, R.A., Petter, A.L., Robinson, R.A.J. & Allen, P.A. (2014). Mass-balance constraints on stratigraphic interpretation of linked alluvial-coastal-shelfal deposits: example from Cretaceous Western Interior Basin, Utah and Colorado, USA. Journal of Sedimentary Research, 84, 935-960.

Haq, B.U. (2018). Jurassic sea-level variations: a reappraisal. GSA Today, 28, 4-10.

Heins, W.A. (2023). Honest bookkeeping for source-to-sink sediment mass-balance analysis with examples from the Angoche margin of Mozambique and the Corsica trough of France. Marine and Petroleum Geology, 153, 106265.

Heins, W.A. & Kairo, S. (2007). Predicting sand character with integrated genetic analysis. In J. Arribas, S. Critelli & M.J. Johnsson (Eds.), Sedimentary provenance and petrogenesis: perspectives from petrography and geochemistry. Geological Society of America, Special Paper 420, 345-379.

Helland-Hansen, W., Ashton, M., Lømo, L. & Steel, R. (1992). Advance and retreat of the Brent delta: recent contributions to the depositional model. In A.C. Morton, R.S. Haszeldine, M.R. Giles & S. Brown (Eds.), Geology of

the Brent Group. Geological Society of London, Special Publication 61, 109-127.

Heller, P.L., Burns, B.A. & Marzo, M. (1993). Stratigraphic solution sets for determining the roles of sediment supply, subsidence, and sea level on transgressions and regressions. Geology, 21, 747-750.

Holbrook, J. & Wanas, H. (2014). A fulcrum approach to assessing source-to-sink mass balance using channel paleohydrologic paramaters derivable from common fluvial data sets with an example from the Cretaceous of Egypt. Journal of Sedimentary Research, 84, 349-372.

Hurst, A. & Morton, A.C. (1988). An application of heavy-mineral analysis to lithostratigraphy and reservoir modelling in the Oseberg Field, northern North Sea. Marine and Petroleum Geology, 5, 157-169.

Husmo, T., Hamar, G.P., Høiland, O., Johannessen, E.P., Rømuld, A., Spencer, A.M. & Titterton, R. (2003). Lower and Middle Jurassic. In D. Evans, C. Graham, A. Armour & P. Bathurst (Eds.) The Millenium Atlas: petroleum geology of the Central and Northern North Sea (pp. 129-155). Geological Society of London.

Johannessen, E.R., Mjøs, R., Renshaw, D., Dalland, A. & Jacobsen, T. (1995). Northern limit of the "Brent delta" at the Tampen Spur - a sequence stratigraphic approach for sandstone prediction. In R.J. Steel, V.L. Felt, E.P. Johannessen & C. Mathieu (Eds.), Sequence stratigraphy on the Northwest European Margin. Norwegian Petroleum Directorate, Special Publication 5, 213-256.

Kieft, R.L., Jackson, C.A-L., Hampson, G.J. & Larsen, E. (2011). Sedimentology and sequence stratigraphy of the Hugin Formation, quadrant 15, Norwegian sector, South Viking Graben. In B.A. Vining & S.C. Pickering (Eds.) Petroleum geology: from mature basins to new frontiers - proceedings of the 7th Petroleum Geology Conference (pp. 157-176). Geological Society of London.

Komar, P.D. (1976). Beach processes and sedimentation. Prentice Hall, New Jersey.

Ksienzyk, A.K., Dunkl, I., Jacobs, J., Fossen, H. & Kohlmann, F. (2014). From orogen to passive margin: constraints from fission track and (U-Th)/He analyses on Mesozoic uplift and fault reactivation in SW Norway. In F. Corfu, D. Gasser & D.M. Chew (Eds.), New perspectives on the Caledonides of Scandinavia and related areas (Vol. 390, pp. 679-702). Geological Society of London, Special Publication 390, 679-702.

Livera, S.E. (1989). Facies associations and sand-body geometries in the Ness Formation of the Brent Group, Brent

Field. In M.K.G. Whateley & K.T. Pickering (Eds.), Deltas: sites and traps for fossil fuels. Geological Society of London, Special Publication 41, 269-286.

Livera, S.E. & Caline, B. (1990). The sedimentology of the Brent Group in the Cormorant Block IV Oilfield. Journal of Petroleum Geology, 13, 367-396.

Løseth, T.M. & Ryseth, A. (2003). A depositional and sequence stratigraphic model for the Rannoch and Etive formations, Oseberg Field, northern North Sea. Norwegian Journal of Geology, 83, 87-106.

Lyster, S.J., Whittaker, A.C., Allison, P.A., Lunt, D.J. & Farnsworth, A. (2020). Predicting sediment discharges and erosion rates in deep time - examples from the late Cretaceous North American continent. Basin Research, 32, 1547-1573.

Mearns, E.W. (1992). Samarium-neodymium isotopic constraints on the provenance of the Brent Group. In A.C. Morton, R.S. Haszeldine, M.R. Giles & S. Brown (Eds.), Geology of the Brent Group. Geological Society of London, Special Publication 61, 213-225.

McLeod, A.E., Dawers, N.H. & Underhill, J.R. (2000). The propogation and linkage of normal faults: insights from the Strathspey-Brent-Statfjord fault array, northern North Sea. Basin Research, 12, 263-284.

McLeod, A.E., Underhill, J.R., Davies, S.J. & Dawers, N.H. (2002). The influence of fault array evolution on synrift sedimentation patterns: controls on deposition in the Strathspey-Brent-Statfjord half graben, northern North Sea. American Association of Petroleum Geologists Bulletin, 86, 1061-1093.

Mearns, E.W. (1992). Samarium-neodymium isotopic constraints on the provenance of the Brent Group. In A.C. Morton, R.S. Haszeldine, M.R. Giles & S. Brown (Eds.), Geology of the Brent Group. Geological Society of London, Special Publication 61, 213-225.

Medvedev, S. & Hartz, E.H. (2015). Evolution of topography of post-Devonian Scandinavia: effects and rates of erosion. Geomorphology, 231, 229-245.

Michael, N.A., Whittaker, A.C. & Allen P.A. (2013). The functioning of sediment routing systems using a mass balance approach: example from the Eocene of the southern Pyrenees. Journal of Geology, 121, 581-606.

Michael, N.A., Whittaker, A.C., Carter, A. & Allen P.A. (2014). Volumetric budget and grain-size fractionation of a geological sediment routing system: Eocene Escanilla Formation, South-Central Pyrenees. Geological Society of America Bulletin, 126, 585-599.

Mitchener, B.C., Lawrence, D.A., Partington, M.A., Bowman, M.B.J. & Gluyas, J. (1992). Brent Group: sequence stratigraphy and regional implications. In A.C. Morton, R.S. Haszeldine, M.R. Giles & S. Brown (Eds.), Geology of the Brent Group. Geological Society of London, Special Publication 61, 45-80.

Morris, J.E., Hampson, G.J. & Maxwell, G. (2003). Controls on facies architecture in the Brent Group, Strathspey Field, UK North Sea: implications for reservoir characterization. Petroleum Geoscience, 9, 209-220.

Morton, A.C. (1985). A new approach to provenance studies: electron microprobe analysis of detrital garnets from Middle Jurassic sandstones of the northern North Sea. Sedimentology, 32, 553-566.

Morton, A.C. (1992). Provenance of Brent Group sandstones: heavy mineral constraints. In A.C. Morton, R.S. Haszeldine, M.R. Giles & S. Brown (Eds.), Geology of the Brent Group. Geological Society of London, Special Publication 61, 227-244.

Morton, A.C., Hallsworth, C. & Chalton, B. (2004). Garnet compositions in Scottish and Norwegian basement terrains: a framework for interpretation of North Sea sandstone provenance. Marine and Petroleum Geology, 21, 393-410.

Muto, T. & Steel, R.J. (1997). The Middle Jurassic Oseberg Delta, northern North Sea: a sedimentological and sequence stratigraphic interpretation. American Association of Petroleum Geologists Bulletin, 81, 1070-1086.

North Sea Transition Authority (2023). Net zero boost as carbon storage licences accepted, https://www.nstauthority.co.uk/news-publications/net-zero-boost-as-carbon-storage-licences-accepted/

Nyberg, B., Helland-Hansen, W., Gawthorpe, R.L., Sandbakken, P., Eide, C.H., Sømme, T., Hadler-Jacobsen, F. & Leiknes, S. (2018). Revisiting morphological relationships of modern source-to-sink segments as a first-order approach to scale ancient sedimentary systems. Sedimentary Geology, 373, 111-133.

Okwara, I.C., Hampson, G.J., Whittaker, A.C., Roberts, G.G. & Ball, P.W. (2023). Source-to-sink mass-balance analysis of an ancient wave-influenced sediment routing system: Middle Jurassic Brent Delta, Northern North Sea,

offshore UK and Norway. Basin Research, 35, 1555-1589.

Olsen, T.R. & Steel, R.J. (1995). Shoreface pinch-out style on the front of the Brent delta in the easterly Tampen Spur area. In R.J. Steel, V.L. Felt, E.P. Johannessen & C. Mathieu (Eds.), Sequence stratigraphy on the Northwest European Margin. Norwegian Petroleum Directorate, Special Publication 5, 273-289.

Palomares, M. & Arribas, J. (1993). Modern stream sands from compound crystalline sources: composition and sand generation index. In M.J. Johnsson & A. Basu (Eds.), Processes controlling the composition of clastic sediment. Geological Society of America, Special Paper 284, 313-320.

Paola, C. & Martin, J.M. (2012). Mass-balance effects in depositional systems. Journal of Sedimentary Research, 82, 435-450.

Partington, M.A., Copestake, P., Mitchener, B.C. & Underhill, J.R. (1993). Biostratigraphic calibration of genetic stratigraphic sequences in the Jurassic–lowermost Cretaceous (Hettangian to Ryazanian) of the North Sea and adjacent areas. In J.R. Parker (Ed.), Petroleum geology of northwest Europe: proceedings of the 4th Petroleum Geology Conference (pp. 371-386). Geological Society of London.

Phillips, T.B., Fazlikhani, H., Gawthorpe, R.L., Fossen, H., Jackson, C.A-L., Bell, R.E., Faleide, J.I. & Rotevatn, A. (2019). The influence of structural inheritance and multiphase extension on rift development, the Northern North Sea. Tectonics, 38, 4099-4126.

Posamentier, H.W. & Vail, P.R. (1988). Eustatic controls on clastic deposition II - sequence and systems tract models. In C.K. Wilgus, B.S. Hastings, C.G.S.C. Kendall, H.W. Posamentier, C.A. Ross & J.C. Van Wagoner (Eds), Sea-level changes - an integrated approach. Society for Sedimentary Geology (SEPM) Special Publication, 42, 125-154.

Prokoph, A., Shields, G.A. & Veizer, J. (2008). Compilation and time-series analysis of a marine carbonate $\delta^{18}O$, $\delta^{13}C$, $^{87}Sr/^{86}Sr$ and $\delta^{34}S$ database through Earth history. Earth-Science Reviews, 87, 113-133.

Quirie, A.K., Schofield, N., Hartley, A., Hole, M.J., Archer, S.G., Underhill, J.R., Watson, D. & Holford, S.P. (2019). The Rattray Volcanics: Mid-Jurassic fissure volcanism in the UK Central North Sea. Journal of the Geological Society, 176, 462-481.

Rattey, R.P. & Hayward, A.B. (1993). Sequence stratigraphy of a failed rift system: the Middle Jurassic to Early Cretaceous basin evolution of the Central and Northern North Sea. In J.R. Parker (Ed.), Petroleum geology of northwest Europe: proceedings of the 4th Petroleum Geology Conference (pp. 215-249). Geological Society of London.

Ravidà, D.C., Caracciolo, L., Heins, W.A. & Stollhofen, H. (2021). Reconstructing environmental signals across the Permian-Triassic boundary in the SE Germanic basin: paleodrainage modelling and quantification of sediment flux. Global and Planetary Change, 206, 103632.

Reynolds, T. (2019). "Grain-size bookkeeping," a new aid for siliciclastic systems with examples from paralic environments. Journal of Sedimentary Research, 89, 976-1016.

Richards, P.C. & Brown, S. (1986). Shoreface storm deposits in the Rannoch Formation (Middle Jurassic), North West Hutton oilfield. Scottish Journal of Geology, 22, 367-375.

Romans, B.W., Castelltort, S., Covault, J.A., Fildani, A. & Walsh, J.P. (2016). Environmental signal propagation in sedimentary systems across timescales. Earth-Science Reviews, 153, 7-29.

Ryseth, A. (1989). Correlation of depositional patterns in the Ness Formation, Oseberg area. In J.D. Collinson (Ed.), Correlation in hydrocarbon exploration (pp. 313-326). Graham and Trotman.

Scott, E.S. (1992). The palaeoenvironments and dynamics of the Rannoch-Etive nearshore and coastal succession, Brent Group, Northern North Sea. In A.C. Morton, R.S. Haszeldine, M.R. Giles & S. Brown (Eds.), Geology of the Brent Group. Geological Society of London, Special Publication 61, 129-147.

Sellwood, B.W. & Valdes, P.J. (2006). Mesozoic climates: general circulation models and the rock record. Sedimentary Geology, 190, 269-287.

Sellwood, B.W. & Valdes, P.J. (2008). Jurassic climates. Proceedings of the Geologists Association, 119, 5-17.

Snedden, J.W., Galloway, W.E., Milliken, K.T., Xu, J., Whiteaker, T. & Blum, M.D. (2018). Validation of empirical source-to-sink scaling relationships in a continental-scale system: the Gulf of Mexico basin Cenozoic record. Geosphere, 14, 768-784.

Sneider, J.S., de Clarens, P. & Vail, P.R. (1995). Sequence stratigraphy of the Middle to Upper Jurassic, Viking Graben, North Sea. In R.J. Steel, V.L. Felt, E.P. Johannessen & C. Mathieu (Eds.), Sequence stratigraphy on the Northwest European Margin. Norwegian Petroleum Directorate, Special Publication 5, 167-197.

Steel, R.J. (1993). Triassic-Jurassic megasequence stratigraphy in the Northern North Sea: rift to post-rift evolution. In J.R. Parker (Ed.), Petroleum geology of northwest Europe: proceedings of the 4th Petroleum Geology Conference (pp. 299-315). Geological Society of London.

Steel, R.J., & Ryseth, A. (1990). The Triassic – Early Jurassic succession in the northern North Sea: megasequence stratigraphy and intra-Triassic tectonics. In R.P.F. Hardman & J. Brooks (Eds.), Tectonic events responsible for Britain's oil and gas reserves. Geological Society of London, Special Publication 55, 139-168.

Strong, N., Sheets, B.A., Hickson, T.A. & Paola, C. (2005). A mass-balance framework for quantifying downstream changes in fluvial architecture. In M. Blum, S. Marriott, S. & S. Leclair (Eds.), Fluvial Sedimentology VII. International Association of Sedimentologists, Special Publication 35, 243–253.

Swift, D.J.P. & Thorne, J.A. (1991). Sedimentation on continental margins, I: a general model for shelf sedimentation. In D.J.P. Swift (Ed.), Shelf sand and sandstone bodies: geometry, facies and sequence stratigraphy. International Association of Sedimentologists, Special Publication 14, 3-31.

Syvitski, J.P.M. & Milliman, J.D. (2007). Geology, geography, and humans battle for dominance over the delivery of fluvial sediment to the coastal ocean. Journal of Geology, 115, 1-19.

Sømme, T.O., Helland-Hansen, W., Martinsen, O.J. & Thurmond, J.B. (2009). Relationships between morphological and sedimentological parameters in source-to-sink systems: a basis for predicting semi-quantitative characteristics in subsurface systems. Basin Research, 21, 361-387.

Torsvik, T.H., Carlos, D., Mosar, J., Cocks, L.R.M. & Malme, T. (2002). Global reconstructions and North Atlantic paleogeography 440 Ma to recent. In E. Eide (Ed.), BATLAS - Mid Norway plate reconstruction atlas with global and Atlantic perspectives (pp. 18-39). Geological Survey of Norway.

Underhill, J.R. & Partington, M.A. (1993). Jurassic thermal doming and deflation in the North Sea: implications of the sequence stratigraphic evidence. In J.R. Parker (Ed.), Petroleum geology of northwest Europe: proceedings of the 4th Petroleum Geology Conference (pp. 337-345). Geological Society of London.

Underhill, J.R. & Partington, M.A. (1994). Use of genetic sequence stratigraphy in defining and determining a regional tectonic control on the "Mid Cimmerian Unconformity": implications for North Sea Basin development and the global sea-level chart. In P. Weimer & H.W. Posamentier (Eds.), Siliciclastic sequence stratigraphy: recent developments and applications. American Association of Petroleum Geologists Memoir *58*, 449-484.

Watkins, S.E., Whittaker, A.C., Bell, R.E., McNeill, L.C., Gawthorpe, R.L., Brooke, S.A. & Nixon, C.W. (2019). Are landscapes buffered to high-frequency climate change? A comparison of sediment fluxes and depositional volumes in the Corinth Rift, central Greece, over the past 130 ky. Geological Society of America Bulletin, 131, 372-388.

Watkins, S.E., Whittaker, A.C., Bell, R.E., Brooke, S.A., Ganti, V., Gawthorpe, R.L., McNeill, L.C. & Nixon, C.W. (2020). Straight from the source's mouth: controls on field-constrained sediment export across the entire active Corinth Rift, central Greece. Basin Research, 32, 1600-1625.

Went, D.J., Hamilton, R.V., Platt, N.H. & Underhill, J.R. (2013). Role of forced regression in controlling Brent Group reservoir architecture and prospectivity in the northern North Sea. Petroleum Geoscience, 19, 307-328.

Whitaker, M.F., Giles, M.R. & Cannon, S.J.C. (1992). Palynological review of the Brent Group, UK sector, North Sea. In A.C. Morton, R.S. Haszeldine, M.R. Giles & S. Brown (Eds.), Geology of the Brent Group. Geological Society of London, Special Publication, 61, 169-202.

Whittaker, A.C., Attal, M. & Allen, P.A. (2010). Characterising the origin, nature and fate of sediment exported from catchments perturbed by active tectonics. Basin Research, 22, 809-828.

Whittaker, A.C., Duller, R.A., Springett, J., Smithells, R.A., Whitchurch, A.L. & Allen, P.A. (2011). Decoding downstream trends in stratigraphic grain-size as a function of tectonic subsidence and sediment supply. Bulletin of Geological Society of America, 123, 1363–1382.

Zanella, E. & Coward, M.P. (2003). Structural framework. In D. Evans, C. Graham, A. Armour & P. Bathurst (Eds.) The Millenium Atlas: petroleum geology of the Central and Northern North Sea (pp. 45-59). Geological Society of London.

Zhang, J., Covault, J., Pyrcz, M., Sharman, G., Carvajal, C., & Milliken, K. (2018). Quantifying sediment supply to continental margins: application to the Paleogene Wilcox Group, Gulf of Mexico. American Association of Petroleum Geologists Bulletin, 102, 1685-1702.

Zhang, J., Burgess, P.M., Granjeon, D., & Steel, R. (2019). Can sediment supply variations create sequences? insights from stratigraphic forward modelling. Basin Research, 31, 274-289.

Ziegler, P.A. (1990). Tectonic and palaeogeographic development of the North Sea rift system. In D.J. Blundell & A.D. Gibbs (Eds.), Tectonic evolution of the North Sea rifts (pp. 1-36). Oxford University Press.

**Table and figure captions**

**Table 1.** Summary of interpreted facies associations, their sediment grain-size characteristics, and their wireline-log signatures (after Supplementary Material of Okwara et al., 2023). Abbreviations for grain-size classes: g – gravel, s – sand, m – mud.

**Figure 1.** (**A**) Schematic illustration of a sediment routing system, which links sediment source areas to depositional sinks, and controls on its development (after Allen and Heller, 2011). These controls force the moving boundaries of the system (e.g. gravel front, sand front, shoreline) to migrate. Stratigraphy results from mass extraction (i.e. to deposition) from the surface sediment flux, and the depositional flux depends on (**B**) the spatial and temporal distribution of accommodation. (**C**) Sediment distribution in a mass balance framework, in which downsystem distance is transformed to the mass extraction domain; the downsystem coordinate $\chi$ shows the depositional mass extracted upsystem, normalised to the total sediment mass deposited in the sediment routing system from source to sink (e.g. Paola and Martin, 2012). The mass balance framework allows sediment routing systems of different scales and spatio-temporal accommodation-space distributions to be compared.

**Figure 2.** (**A**) Unrestored Middle Jurassic palaeogeographic reconstruction of the North Sea (Ziegler, 1990; Torsvik et al., 2002). (**B**) Restored Middle Jurassic palaeogeographic reconstruction of the Northern North Sea showing palaeo-landmasses and basins (Ziegler, 1990). Note the extent of the proto-Viking Graben (VG) and sediment input into the basin from the Shetland Platform (SP), Norwegian Landmass (NL), and Mid-North Sea High (MNSH). Additional tectonic elements include the Central North Sea (CNS), Egersund Basin (EB), Faroes-Shetland Basin (FSB), Horda Platform (HP), London-Brabant Massif (LBM), Moray Firth Basin (MFB), Møre Basin (MB), Rhenish Massif (RM), Rockall Basin (RB), South Permian Basin (SPB), Unst Basin (UB), West Hebrides Basin (WHP). The mapped extent of the subcrop beneath the 'Mid-Cimmerian Unconformity', which formed due to initiation of the

MNSH uplift (Underhill and Partington, 1993) is shown. Depocentres supplied by abundant clastic sediment occur in the Faroes-Shetland Basin (FSB), South Permian Basin (SPB), Egersund Basin (EB) and in northern Germany, in addition to the 'Brent Delta' depocentre in the Viking Graben (VG) and Horda Platform (HP). (**C**) Simplified lithostratigraphic column for the proto-Viking Graben (Fig. 2B) highlighting the main phases of structural evolution in relation to deposition of the Brent Delta sediment routing system(s) (Fig. 3).

**Figure 3.** Sequence stratigraphic framework for the 'Brent Delta' synthesised from various published references (Deegan and Scull, 1977; Mitchener et al., 1992; Partington et al., 1993; Sneider et al., 1995; Johannessen et al., 1995; Fjellanger et al., 1996; Hampson et al., 2004). The Aalenian to Bathonian genetic sequences (J22, J24, J26 and J32) of Mitchener et al. (1992) are used in this study. Possible tectonic drivers in the Shetland Platform, Norwegian Landmass, and Mid-North Sea High source regions and depositional sink, climate (Prokoph et al., 2008), eustatic sea-level change (Haq, 2018), and estimated relative contributions from the source regions to the sediment budget of the 'Brent Delta' sediment routing system(s), based on the relative proportion of detrital garnet compositional suites (Morton, 1992), are shown (after Okwara et al., 2023). Facies Association (FAs) in each Gross Depositional Environment are summarised in Table 1.

**Figure 4.** Maps locating: (**A**) the study area (Fig. 4B); and (**B**) wells in the study dataset (numbered according to Table S1), and regional stratigraphic correlation panels (Fig. S2). To aid clarify, two west-east-oriented (transverse) correlation panels (Fig. S2A, B) are shown in blue and one north-south-oriented (axial) correlation panel (Fig. S2C) is shown in red. Wells in the study dataset and previously published interpretations of these wells are summarised in Table S1.

**Figure 5.** (**A**) Isopach map and (**B**) palaeogeographic reconstruction for genetic sequence J22 (Fig. 3), during maximum progradation of the eastward prograding 'Broom Delta' and westward prograding 'Oseberg Delta' (after Okwara et al., 2023 and references therein). Maps show the extent of deposition prior to Late Jurassic erosion (dotted lines; Husmo et al., 2003) and the location of Shetland Platform, Norwegian Landmass and Mid-North Sea High source areas (Ziegler 1990; Underhill and Partington, 1993). Facies Association (FAs) in each Gross Depositional Environment (Fig. 5B) are summarised in Table 1 and illustrated in Supplementary Figures S1 and S2. Cored and uncored wells in the study dataset are shown as green and red circles, respectively. Red rectangles indicate the areas for which sediment masses have been calculated for three distinct sediment routing systems, with wells in each area projected into a transverse (Fig. 10A, B) or axial transect (Fig. 10C) through the sediment routing system.

**Figure 6.** (**A**) Isopach map and (**B**) palaeogeographic reconstruction for genetic sequence J24 (Fig. 3), during maximum progradation of the northward-prograding 'Brent Delta' (after Okwara et al., 2023 and references therein). Maps show the extent of deposition prior to Late Jurassic erosion (dotted lines; Husmo et al., 2003) and the location of Shetland Platform, Norwegian Landmass and Mid-North Sea High source areas (Ziegler 1990; Underhill and Partington, 1993). Facies Association (FAs) in each Gross Depositional Environment (Fig. 6B) are summarised in Table 1 and illustrated in Supplementary Figures S1 and S2. Cored and uncored wells in the study dataset are shown as green and red circles, respectively. The red rectangle indicates the area for which sediment mass has been calculated for a combined sediment routing system, with wells in the area projected into an axial transect (Fig. 11) through the sediment routing system.

**Figure 7.** (**A**) Isopach map and (**B**) palaeogeographic reconstruction for genetic sequence J26 (Fig. 3), during aggradation of the 'Brent Delta' (after Okwara et al., 2023 and references therein). Maps show the extent of deposition prior to Late Jurassic erosion (dotted lines; Husmo et al., 2002) and the location of Shetland Platform, Norwegian Landmass and Mid-North Sea High source areas (Ziegler 1990; Underhill and Partington, 1993). Facies Association (FAs) in each Gross Depositional Environment (Fig. 7B) are summarised in Table 1 and illustrated in Supplementary Figures S1 and S2. Cored and uncored wells in the study dataset are shown as green and red circles, respectively. The red rectangle indicates the area for which sediment mass has been calculated for a combined sediment routing system, with wells in the area projected into an axial transect (Fig. 12) through the sediment routing system.

**Figure 8.** (**A**) Isopach map and (**B**) palaeogeographic reconstruction for genetic sequence J32 (Fig. 3), during transgression of the 'Brent Delta' and shoreline retreat to the western, eastern and southern basin margins (after Okwara et al., 2023 and references therein). Maps show the extent of deposition prior to Late Jurassic erosion (dotted lines; Husmo et al., 2003) and the location of Shetland Platform, Norwegian Landmass and Mid-North Sea High source areas (Ziegler 1990; Underhill and Partington, 1993). Facies Association (FAs) in each Gross Depositional Environment (Fig. 8B) are summarised in Table 1 and illustrated in Supplementary Figures S1 and S2. Cored and uncored wells in the study dataset are shown as green and red circles, respectively. Red rectangles indicate the areas for which sediment masses have been calculated for three distinct sediment routing systems, with wells in each area projected into a transverse (Fig. 13A, B) or axial transect (Fig. 13C) through the sediment routing system.

**Figure 9.** (**A**) Net-depositional sediment budget for the four genetic sequences of the 'Brent Delta' sediment routing system(s) (Fig. 3; after Okwara et al., 2023). Genetic sequences are shown from oldest (J22, left) to youngest (J32, right). Black line shows the median (P50) value and grey shading shows the 10th to 90th percentile range (P10-P90)

for each genetic sequence, accounting for uncertainties in sediment volumes, volume-to-mass conversions and genetic sequence durations (Okwara et al., 2023). (**B**) Proportion of grain-size classes (gravel, sandstone and mudstone) by mass in genetic sequences J22, J24, J26 and J32, based on mapped sediment volumes (Figs. 5-8) that are subdivided into facies proportions in 84 representative wells (Figs. 4, S1; see Supplementary Material for details). Each facies is assigned a specific grain size composition (Table 1), and volume-to-mass conversions based on density log data are applied to each grain-size class (2400 kg $m^{-3}$ = gravel conglomerate and sandstone bulk density, 2500 kg $m^{-3}$ = mudstone bulk density; Okwara et al., 2023).

**Figure 10.** Downsystem variations in (**A-C**) percentage-thickness of gravel, sandstone and mudstone, and (**D-F**) percentage-thickness of coastal-plain, marginal-marine and shallow-marine sandstones for genetic sequence J22 (cf. Figs. 5, S2A-C) in the study well database (Fig. 4), as a function of sediment mass extracted ($\chi$) (Equation 1, Fig. 1). Downsystem variations are shown for: (**A, D**) transverse transect for western basin margin, sourced from Shetland Platform; (**B, E**) transverse transect for eastern basin margin, sourced from Norwegian Landmass; and (**C, F**) axial transect for southern basin margin, sourced from Mid-North Sea High (Fig. 5). Each point in the plots represents the mean value for a group of wells located at a specific downsystem distance, with the number of wells in the group indicated at the top of the plot (e.g. "n=3"). The vertical error bar for each point shows the variation in percentage-thickness values between wells in the group.

**Figure 11.** Downsystem variations in (**A**) percentage-thickness of gravel, sandstone and mudstone, and (**B**) percentage-thickness of coastal-plain, marginal-marine and shallow-marine sandstones for genetic sequence J24 (cf. Figs. 6, S2C) in the study well database (Fig. 4), as a function of sediment mass extracted ($\chi$) (Equation 1, Fig. 1). Downsystem variations are shown for axial transect along basin centre, sourced from Shetland Platform, Norwegian Landmass and Mid-North Sea High (Fig. 6). Each point in the plots represents the mean value for a group of wells located at a specific downsystem distance, with the number of wells in the group indicated at the top of the plot (e.g. "n=3"). The vertical error bar for each point shows the variation in percentage-thickness values between wells in the group. Key as for Figure 10.

**Figure 12.** Downsystem variations in (A) percentage-thickness of gravel, sandstone and mudstone, and (B) percentage-thickness of coastal-plain, marginal-marine and shallow-marine sandstones for genetic sequence J26 (cf. Figs. 7, S2C) in the study well database (Fig. 4), as a function of sediment mass extracted ($\chi$) (Equation 1, Fig. 1). Downsystem variations are shown for axial transect along basin centre, sourced from Shetland Platform, Norwegian Landmass and Mid-North Sea High (Fig. 7). Each point in the plots represents the mean value for a group of wells located at a specific downsystem distance, with the number of wells in the group indicated at the

top of the plot (e.g. "n=3"). The vertical error bar for each point shows the variation in percentage-thickness values between wells in the group. Key as for Figure 10.

**Figure 13.** Downsystem variations in (**A-C**) percentage-thickness of gravel, sandstone and mudstone, and (**D-F**) percentage-thickness of coastal-plain, marginal-marine and shallow-marine sandstones for genetic sequence J32 (cf. Figs. 8, S2A-C) in the study well database (Fig. 4), as a function of sediment mass extracted ($\chi$) (Equation 1, Fig. 1). Downsystem variations are shown for: (**A, D**) transverse transect for western basin margin, sourced from Shetland Platform; (**B, E**) transverse transect for eastern basin margin, sourced from Norwegian Landmass; and (**C, F**) axial transect for southern basin margin, sourced from Mid-North Sea High (Fig. 8). Each point in the plots represents the mean value for a group of wells located at a specific downsystem distance, with the number of wells in the group indicated at the top of the plot (e.g. "n=3"). The vertical error bar for each point shows the variation in percentage-thickness values between wells in the group. Key as for Figure 10.

**Figure 14.** Conceptual model synthesising sediment source regions, sediment influxes and effluxes, depositional environments, and downsystem variations in gravel (orange), sandstone (yellow) and mudstone (grey) in the axial 'Brent Delta' sediment routing system. See text for discussion.

***Table 1.*** *Summary of interpreted facies associations, their sediment grain-size characteristics, and their wireline-log signatures (after Supplementary Material of Okwara et al., 2023). Abbreviations for grain-size classes: g – gravel, s – sand, m – mud.*

| Facies association | Lithostratigraphic distribution | Sedimentological description | Proportion of grain-size class | Wireline log response |
|---|---|---|---|---|
| **1. Coastal plain** | | | | |
| 1.1. Fluvial channel | Ness Fm.; Sleipner Fm.; Bruce 'C' Sands | Poorly to moderately sorted, fining-upward, fine- to coarse-grained sandstone (2-8 m thick). Pebble lag above erosional base. Cross-beds and asymmetrical ripples. Bioturbation absent to low in intensity. | g - 5%; s - 90%; m - 5% | Low, upward-increasing gamma ray (20-40 API), moderate sonic (60-80 μs/ft), moderate to high density (2.4-2.6 g/cm$^3$), low neutron (2-25 p.u). |
| 1.2. Floodplain | Ness Fm.; Sleipner Fm. | Mudstone (2-10 m thick) interbedded with very fine- to medium-grained sandstone. Plant root traces common. Bioturbation absent to moderate in intensity. | g - 0%; s - 20%; m - 80% | Variable, high gamma ray (60-90 API), high sonic (80-100 μs/ft), moderate to high density (2.35-2.7 g/cm$^3$), moderate to high neutron (15-50p.u.). |
| 1.3. Swamp | Ness Fm.; Sleipner Fm.; Bruce B-C Coal | Coal and carbonaceous shale (<1 m thick). Bioturbation absent. | *In situ* biogenic accumulation | Low gamma ray (20-35 API), very high sonic (110-130 μs/ft), low density (1.6-1.8 g/cm$^3$), high neutron (50-60 p.u.). |
| **2. Marginal marine** | | | | |
| 2.1. Lagoon | Ness Fm.; Sleipner Fm. | Mudstone (1-4 m thick) with rare beds of very fine- to fine-grained sandstone. Parallel lamination, symmetrical and asymmetrical ripples. Rare hummocky cross-stratification. Sparse to moderate bioturbation intensity. | g - 0%; s - 20%; m - 80% | High gamma ray (70-80 API), moderate sonic (80-90 μs/ft), high density (2.6-2.65 g/cm$^3$), moderate to high neutron (30-45 p.u.). |
| 2.2. Fluvio-tidal / estuarine channel and fan delta | Broom Fm.; Oseberg Fm.; Etive Fm.; Ness Fm.; Tarbert Fm.; Bruce 'B' Sands | Moderately to well-sorted, medium- to very coarse-grained sandstone (10-25 m thick) with sharp or erosional base. Cross-beds, asymmetrical ripples, mud drapes. Bioturbation is generally low to moderate in intensity. | g - 5%; s - 90%; m - 5% | Low to moderate, uniform to upward-increasing gamma ray (15-45 API), moderate to high sonic (60-95 μs/ft), moderate to high density (2.2-2.65 g/cm$^3$), low to moderate neutron (0.5-25 p.u.). |
| 2.3. Bay-head and lagoonal delta | Ness Fm.; Sleipner Fm. | Very fine- to medium-grained, well to moderately sorted sandstone (3-7 m thick) usually interbedded with lagoon mudstone (FA 2.1). Symmetrical and asymmetrical ripples, low-angle cross-lamination, climbing asymmetrical ripples. Generally sparse to moderate bioturbation intensity. | g - 0%; s - 80%; m - 20% | Typically upward-decreasing gamma ray (20-70 API), moderate to high sonic (70-90 μs/ft), moderate density (2.3-2.55 g/cm$^3$), low to moderate neutron (6-28 p.u.). |
| **3. Shallow marine to shelf** | | | | |
| 3.1. Weakly wave-influenced (bioturbated) shoreface | Broom Fm.; Oseberg Fm.; Tarbert Fm. | Moderately to well-sorted, coarsening-upward, fine- to coarse-grained sandstone (10-20 m thick). Planar-parallel lamination and low-angle cross-lamination. Moderate to high bioturbation intensity in lower parts and low bioturbation intensity in upper parts of coarsening-upward units. | g - 0%; s - 100%; m - 0% | Moderate, upward-decreasing gamma ray (40-70 API), moderate sonic (75-85 μs/ft), moderate to high density (2.35-2.62 g/cm$^3$), moderate neutron (20-30 p.u.). |
| 3.2. Wave-dominated upper shoreface and barrier bar | Etive Fm.; Hugin Fm.; Tarbert Fm. | Well-sorted, coarsening-upward, fine- to medium-grained sandstone (8-35 m thick). May appear structureless, but planar and trough cross-beds, asymmetrical ripples, planar-parallel lamination, low angle cross-lamination and dewatering structures occur. Absent to low bioturbation intensity. | g - 0%; s - 100%; m - 0% | Low, upward-decreasing gamma ray (10-35 API), moderate to high sonic (70-90 μs/ft), moderate density (2.2-2.6 g/cm$^3$), low to moderate neutron (3-30 p.u.). |
| 3.3. Proximal lower shoreface | Rannoch Fm.; Hugin Fm.; Bruce 'A' Sands | Coarsening-upward succession of micaceous, well-sorted, fine- to lower medium-grained sandstone (5-25 m thick). Low-angle and hummocky cross-stratification, minor symmetrical and asymmetrical ripple cross-lamination. Bioturbation intensity is sparse to low. | g - 0%; s - 100%; m - 0% | Moderate, upward-increasing gamma ray (40-70 API), moderate sonic (70-85 μs/ft), variable density (2.3-2.7 g/cm$^3$), moderate neutron (20-36 p.u.). |
| 3.4. Distal lower shoreface and offshore | lower Rannoch Fm.; Heather Fm. | Dominantly mudstone, may be interbedded with pinstripe laminae and thin beds of very fine- to fine-grained sandstone. Pyrite nodules and scattered shells occur. Bioturbation intensity is moderate to intense. | g - 0%; s - 0%; m - 100% | High gamma ray (55-120 API), moderate to high sonic (80-95 μs/ft), high density (2.5-2.65 g/cm$^3$), variable neutron porosity (12-40 p.u.). |

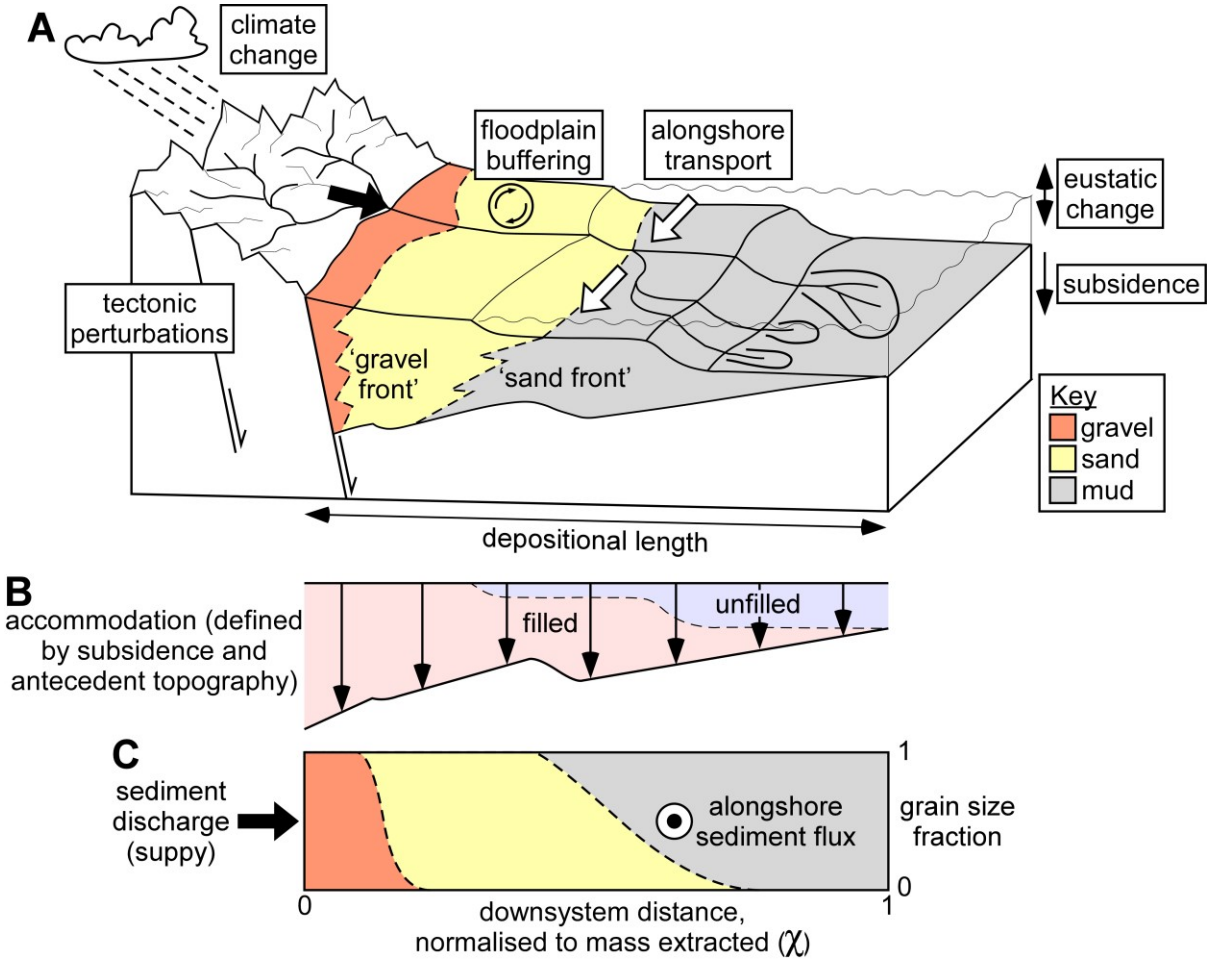


**Figure 1.** (**A**) Schematic illustration of a sediment routing system, which links sediment source areas to depositional sinks, and controls on its development (after Allen and Heller, 2011). These controls force the moving boundaries of the system (e.g. gravel front, sand front, shoreline) to migrate. Stratigraphy results from mass extraction (i.e. to deposition) from the surface sediment flux, and the depositional flux depends on (**B**) the spatial and temporal distribution of accommodation. (**C**) Sediment distribution in a mass balance framework, in which downsystem distance is transformed to the mass extraction domain; the downsystem coordinate $\chi$ shows the depositional mass extracted upsystem, normalised to the total sediment mass deposited in the sediment routing system from source to sink (e.g. Paola and Martin, 2012). The mass balance framework allows sediment routing systems of different scales and spatio-temporal accommodation-space distributions to be compared.

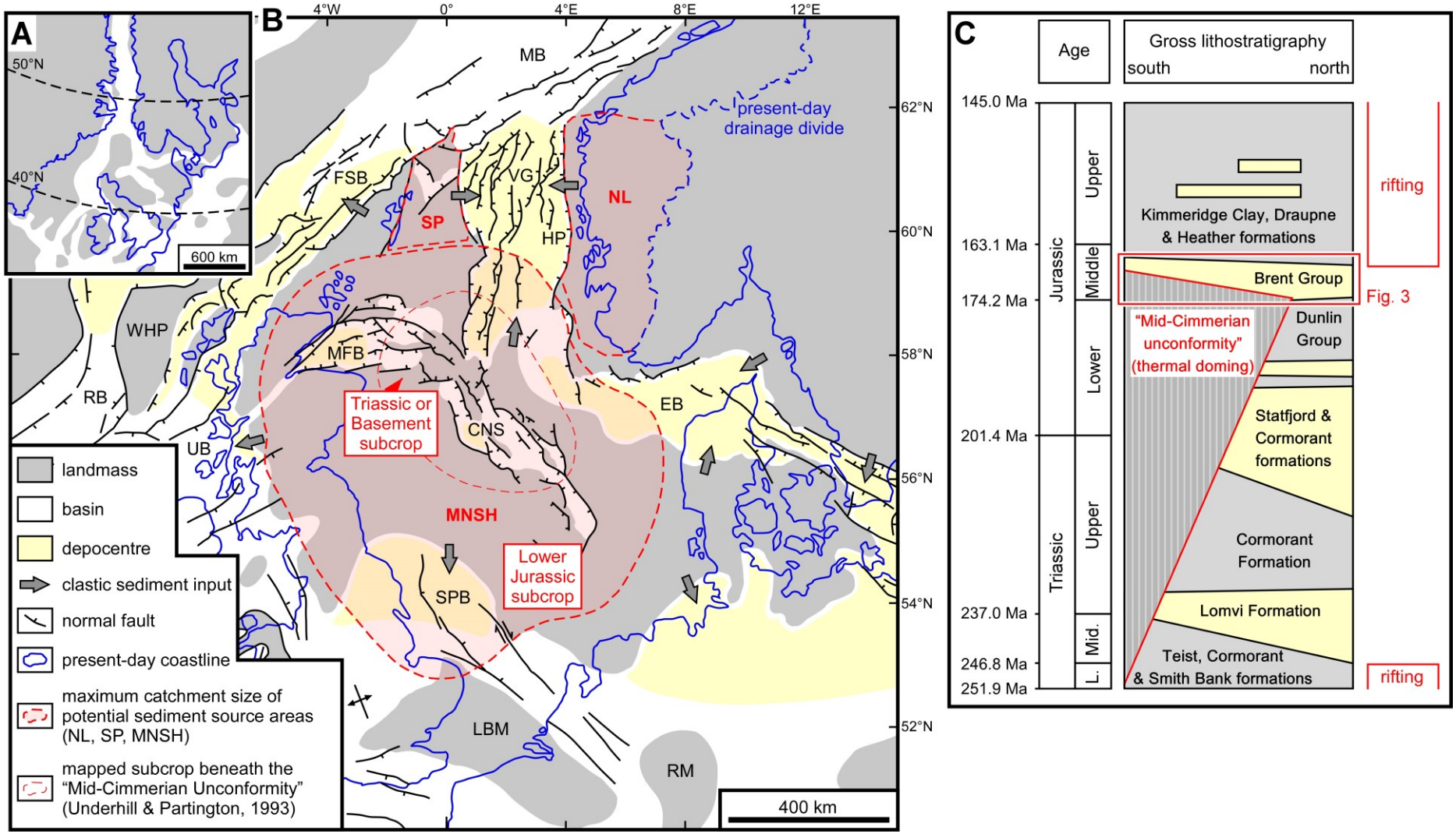
A
50°N
40°N
600 km
B
4°W
0°
4°E
8°E
12°E
62°N
60°N
58°N
56°N
54°N
52°N
MB
present-day
drainage divide
FSB
VG
NL
SP
HP
WHP
MFB
RB
Triassic or
Basement
subcrop
CNS
EB
UB
MNSH
Lower
Jurassic
subcrop
SPB
LBM
RM
400 km
landmass
basin
depocentre
clastic sediment input
normal fault
present-day coastline
maximum catchment size of
potential sediment source areas
(NL, SP, MNSH)
mapped subcrop beneath the
"Mid-Cimmerian Unconformity"
(Underhill & Partington, 1993)
C
Age
Gross lithostratigraphy
south
north
145.0 Ma
163.1 Ma
174.2 Ma
201.4 Ma
237.0 Ma
246.8 Ma
251.9 Ma
Jurassic
Triassic
Upper
Middle
Lower
Upper
Mid.
L.
Kimmeridge Clay, Draupne
& Heather formations
Brent Group
"Mid-Cimmerian
unconformity"
(thermal doming)
Dunlin
Group
Statfjord &
Cormorant
formations
Cormorant
Formation
Lomvi Formation
Teist, Cormorant
& Smith Bank formations
rifting
Fig. 3
rifting

**Figure 2.** (**A**) Unrestored Middle Jurassic palaeogeographic reconstruction of the North Sea (Ziegler, 1990; Torsvik et al., 2002). (**B**) Restored Middle Jurassic palaeogeographic reconstruction of the Northern North Sea showing palaeo-landmasses and basins (Ziegler, 1990). Note the extent of the proto-Viking Graben (VG) and sediment input into the basin from the Shetland Platform (SP), Norwegian Landmass (NL), and Mid-North Sea High (MNSH). Additional tectonic elements include the Central North Sea (CNS), Egersund Basin (EB), Faroes-Shetland Basin (FSB), Horda Platform (HP), London-Brabant Massif (LBM), Moray Firth Basin (MFB), Møre Basin (MB), Rhenish Massif (RM), Rockall Basin (RB), South Permian Basin (SPB), Unst Basin (UB), West Hebrides Basin (WHP). The mapped extent of the subcrop beneath the 'Mid-Cimmerian Unconformity', which formed due to initiation of the MNSH uplift (Underhill and Partington, 1993) is shown. Depocentres supplied by abundant clastic sediment occur in the Faroes-Shetland Basin (FSB), South Permian Basin (SPB), Egersund Basin (EB) and in northern Germany, in addition to the 'Brent Delta' depocentre in the Viking Graben (VG) and Horda Platform (HP). (**C**) Simplified lithostratigraphic column for the proto-Viking Graben (Fig. 2B) highlighting the main phases of structural evolution in relation to deposition of the Brent Delta sediment routing system(s) (Fig. 3).

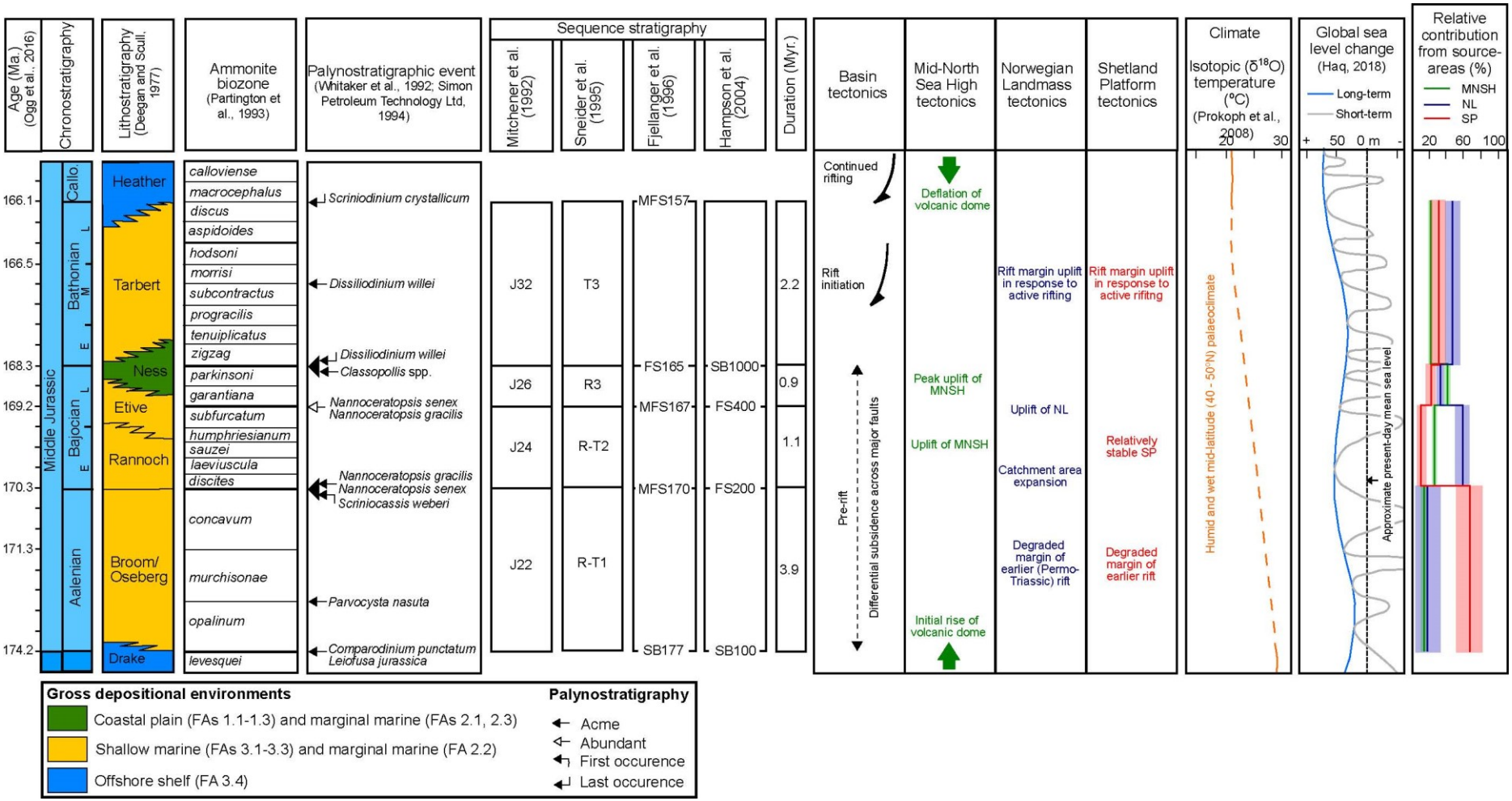


**Figure 3.** Sequence stratigraphic framework for the 'Brent Delta' synthesised from various published references (Deegan and Scull, 1977; Mitchener et al., 1992; Partington et al., 1993; Sneider et al., 1995; Johannessen et al., 1995; Fjellanger et al., 1996; Hampson et al., 2004). The Aalenian to Bathonian genetic sequences (J22, J24, J26 and J32) of Mitchener et al. (1992) are used in this study. Possible tectonic drivers in the Shetland Platform, Norwegian Landmass, and

Mid-North Sea High source regions and depositional sink, climate (Prokoph et al., 2008), eustatic sea-level change (Haq, 2018), and estimated relative contributions from the source regions to the sediment budget of the 'Brent Delta' sediment routing system(s), based on the relative proportion of detrital garnet compositional suites (Morton, 1992), are shown (after Okwara et al., 2023). Facies Association (FAs) in each Gross Depositional Environment are summarised in Table 1.

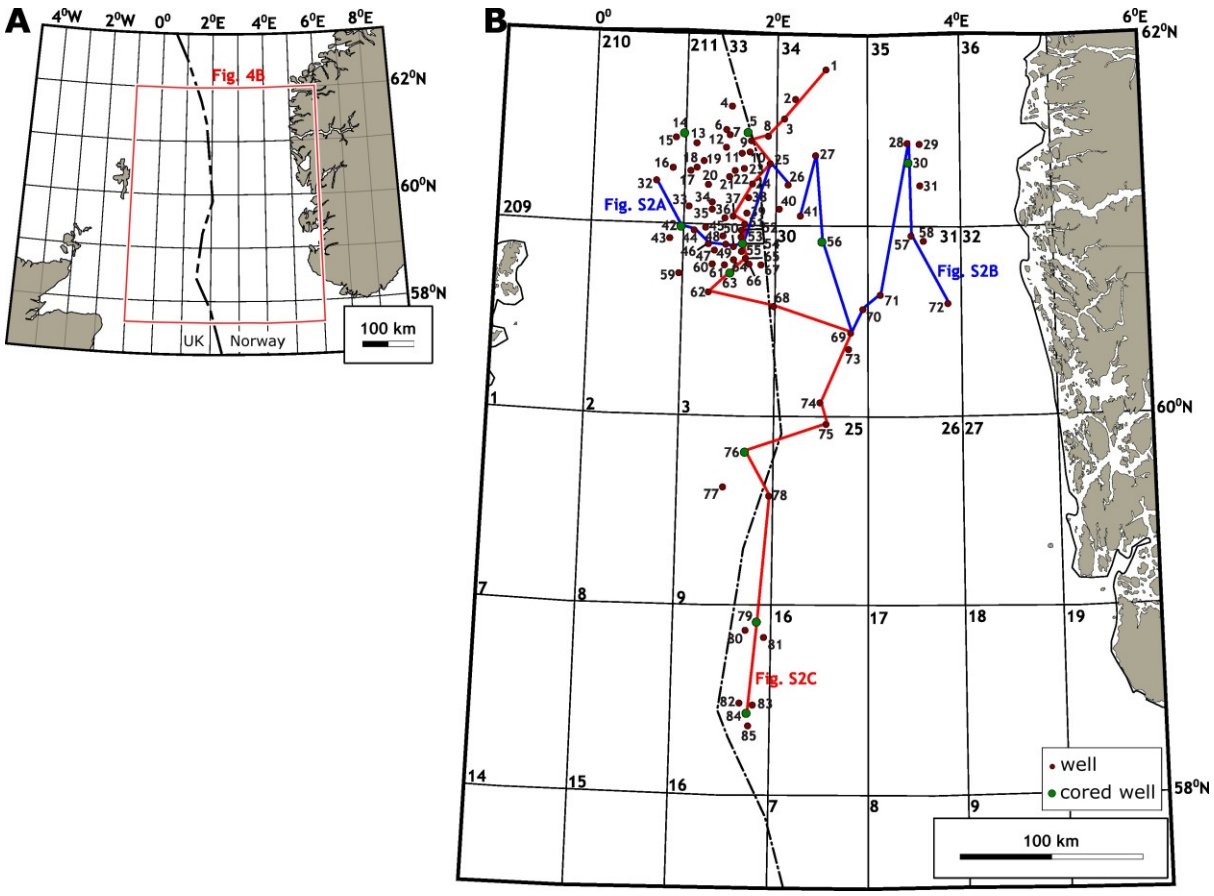


**Figure 4.** Maps locating: (**A**) the study area (Fig. 4B); and (**B**) wells in the study dataset (numbered according to Table S1), and regional stratigraphic correlation panels (Fig. S2). To aid clarify, two west-east-oriented (transverse) correlation panels (Fig. S2A, B) are shown in blue and one north-south-oriented (axial) correlation panel (Fig. S2C) is shown in red. Wells in the study dataset and previously published interpretations of these wells are summarised in Table S1.

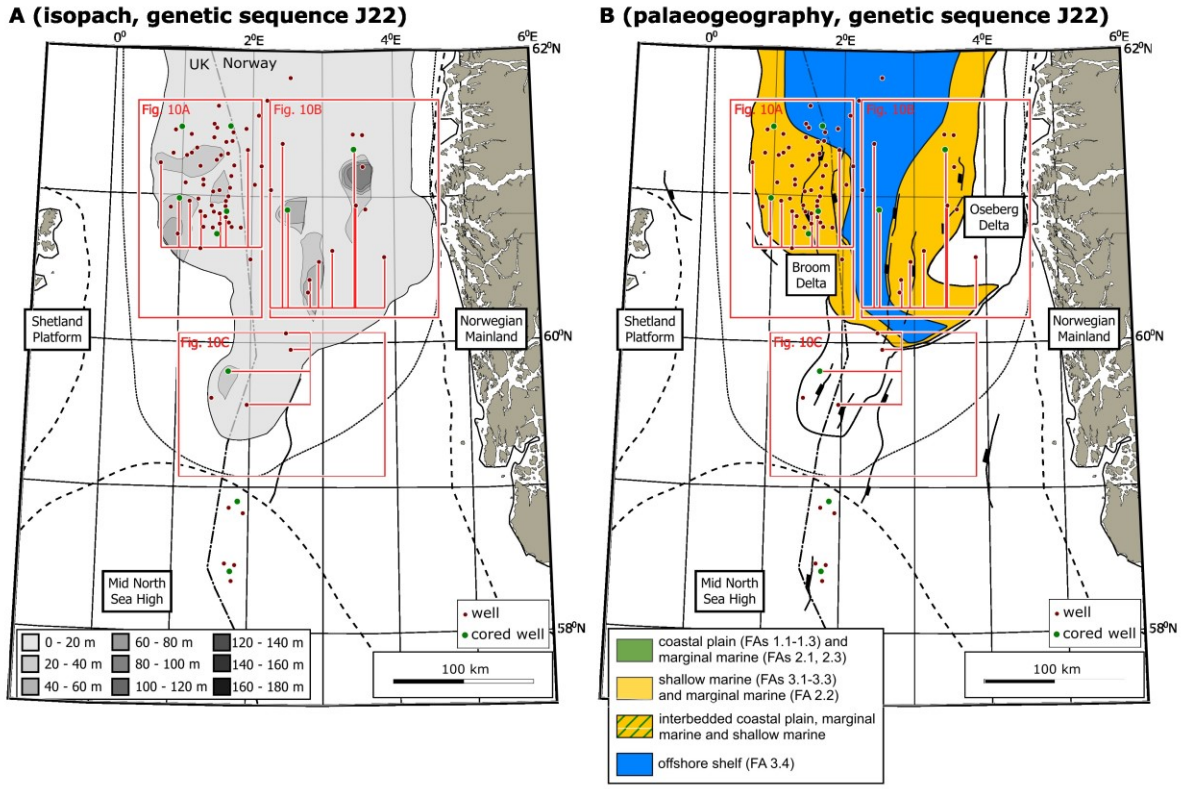


**Figure 5.** (**A**) Isopach map and (**B**) palaeogeographic reconstruction for genetic sequence J22 (Fig. 3), during maximum progradation of the eastward prograding 'Broom Delta' and westward prograding 'Oseberg Delta' (after Okwara et al., 2023 and references therein). Maps show the extent of deposition prior to Late Jurassic erosion (dotted lines; Husmo et al., 2003) and the location of Shetland Platform, Norwegian Landmass and Mid-North Sea High source areas (Ziegler 1990; Underhill and Partington, 1993). Facies Association (FAs) in each Gross Depositional Environment (Fig. 5B) are summarised in Table 1 and illustrated in Supplementary Figures S1 and S2. Cored and uncored wells in the study dataset are shown as green and red circles, respectively. Red rectangles indicate the areas for which sediment masses have been calculated for three distinct sediment routing systems, with wells in each area projected into a transverse (Fig. 10A, B) or axial transect (Fig. 10C) through the sediment routing system.

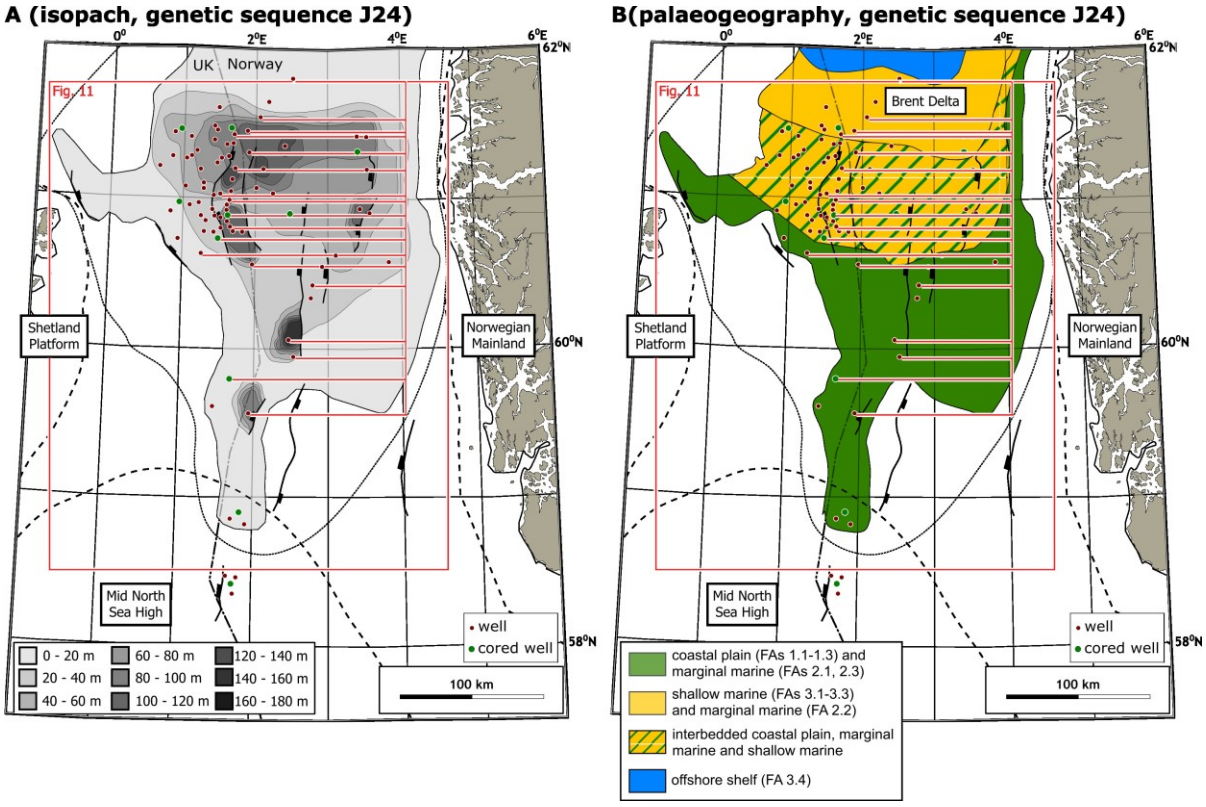


**Figure 6.** (**A**) Isopach map and (**B**) palaeogeographic reconstruction for genetic sequence J24 (Fig. 3), during maximum progradation of the northward-prograding 'Brent Delta' (after Okwara et al., 2023 and references therein). Maps show the extent of deposition prior to Late Jurassic erosion (dotted lines; Husmo et al., 2003) and the location of Shetland Platform, Norwegian Landmass and Mid-North Sea High source areas (Ziegler 1990; Underhill and Partington, 1993). Facies Association (FAs) in each Gross Depositional Environment (Fig. 6B) are summarised in Table 1 and illustrated in Supplementary Figures S1 and S2. Cored and uncored wells in the study dataset are shown as green and red circles, respectively. The red rectangle indicates the area for which sediment mass has been calculated for a combined sediment routing system, with wells in the area projected into an axial transect (Fig. 11) through the sediment routing system.

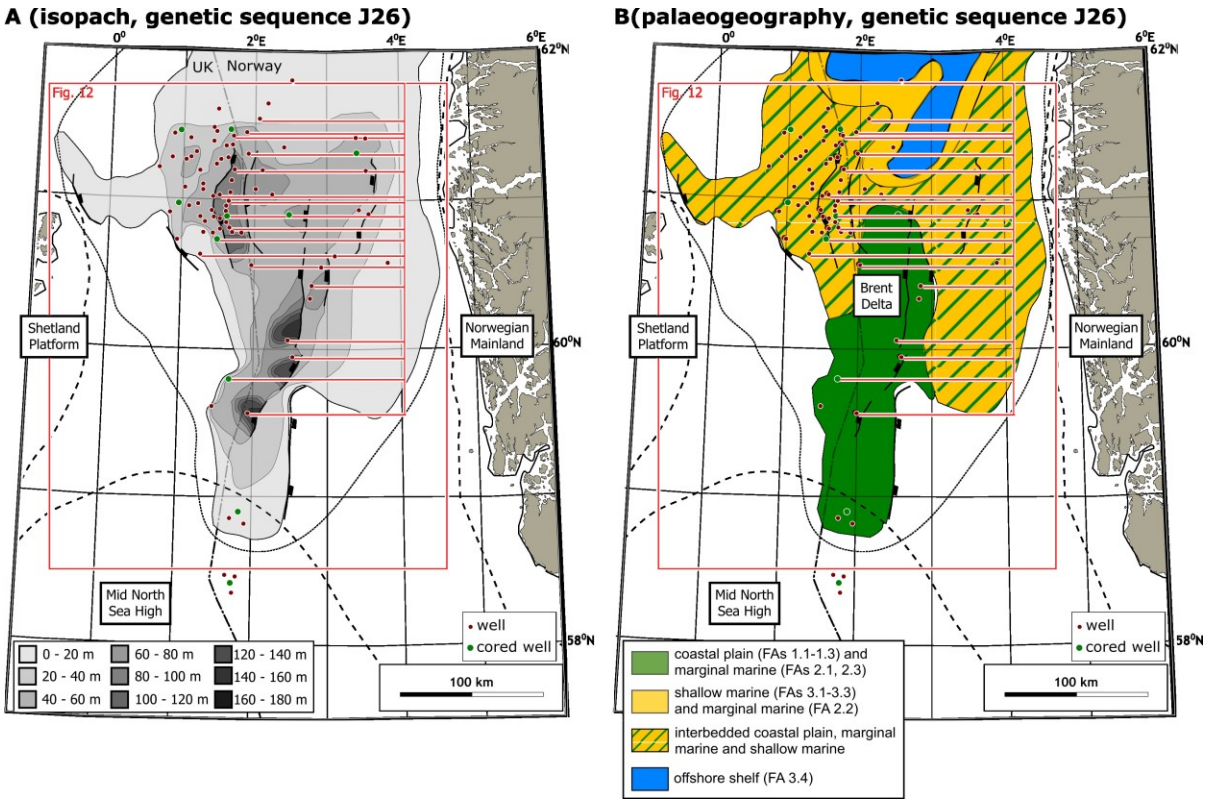


**Figure 7.** (**A**) Isopach map and (**B**) palaeogeographic reconstruction for genetic sequence J26 (Fig. 3), during aggradation of the 'Brent Delta' (after Okwara et al., 2023 and references therein). Maps show the extent of deposition prior to Late Jurassic erosion (dotted lines; Husmo et al., 2002) and the location of Shetland Platform, Norwegian Landmass and Mid-North Sea High source areas (Ziegler 1990; Underhill and Partington, 1993). Facies Association (FAs) in each Gross Depositional Environment (Fig. 7B) are summarised in Table 1 and illustrated in Supplementary Figures S1 and S2. Cored and uncored wells in the study dataset are shown as green and red circles, respectively. The red rectangle indicates the area for which sediment mass has been calculated for a combined sediment routing system, with wells in the area projected into an axial transect (Fig. 12) through the sediment routing system.

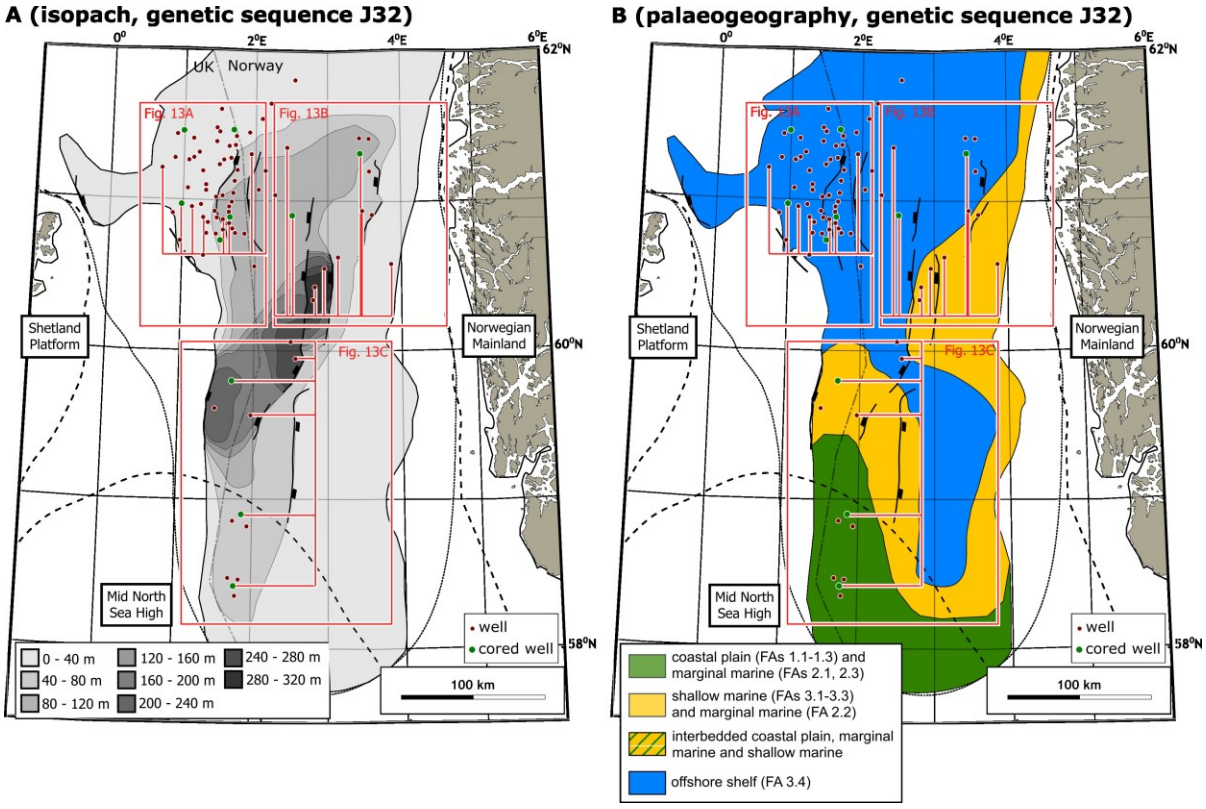


**Figure 8.** (**A**) Isopach map and (**B**) palaeogeographic reconstruction for genetic sequence J32 (Fig. 3), during transgression of the 'Brent Delta' and shoreline retreat to the western, eastern and southern basin margins (after Okwara et al., 2023 and references therein). Maps show the extent of deposition prior to Late Jurassic erosion (dotted lines; Husmo et al., 2003) and the location of Shetland Platform, Norwegian Landmass and Mid-North Sea High source areas (Ziegler 1990; Underhill and Partington, 1993). Facies Association (FAs) in each Gross Depositional Environment (Fig. 8B) are summarised in Table 1 and illustrated in Supplementary Figures S1 and S2. Cored and uncored wells in the study dataset are shown as green and red circles, respectively. Red rectangles indicate the areas for which sediment masses have been calculated for three distinct sediment routing systems, with wells in each area projected into a transverse (Fig. 13A, B) or axial transect (Fig. 13C) through the sediment routing system.

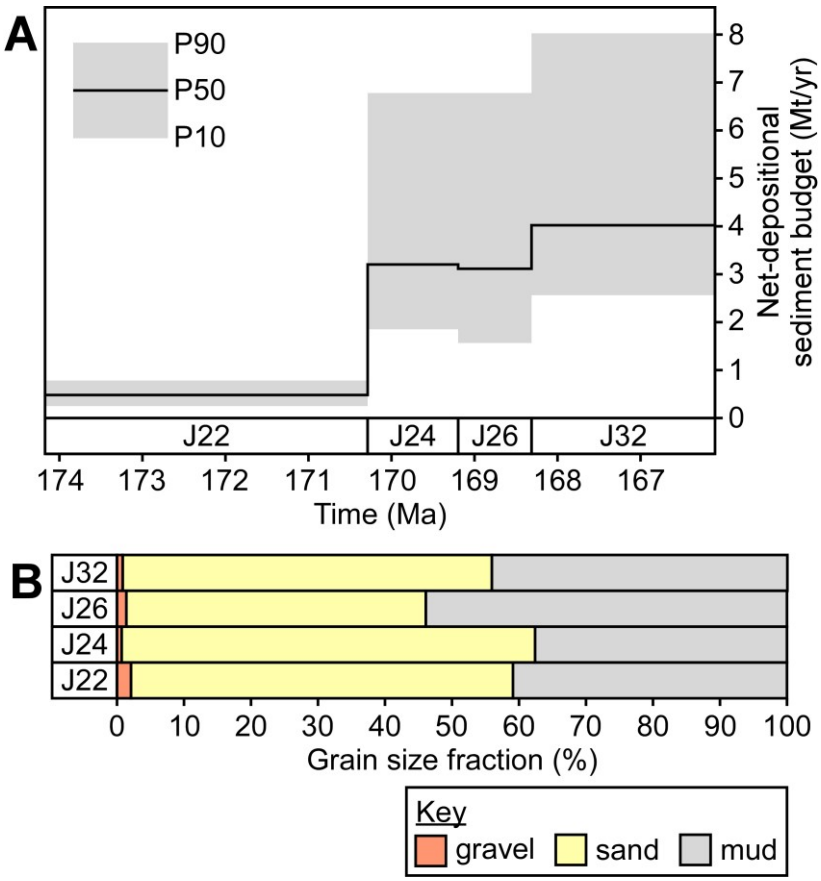


**Figure 9.** (**A**) Net-depositional sediment budget for the four genetic sequences of the 'Brent Delta' sediment routing system(s) (Fig. 3; after Okwara et al., 2023). Genetic sequences are shown from oldest (J22, left) to youngest (J32, right). Black line shows the median (P50) value and grey shading shows the 10th to 90th percentile range (P10-P90) for each genetic sequence, accounting for uncertainties in sediment volumes, volume-to-mass conversions and genetic sequence durations (Okwara et al., 2023). (**B**) Proportion of grain-size classes (gravel, sandstone and mudstone) by mass in genetic sequences J22, J24, J26 and J32, based on mapped sediment volumes (Figs. 5-8) that are subdivided into facies proportions in 84 representative wells (Figs. 4, S1; see Supplementary Material for details). Each facies is assigned a specific grain size composition (Table 1), and volume-to-mass conversions based on density log data are applied to each grain-size class (2400 kg $m^{-3}$ = gravel conglomerate and sandstone bulk density, 2500 kg $m^{-3}$ = mudstone bulk density; Okwara et al., 2023).

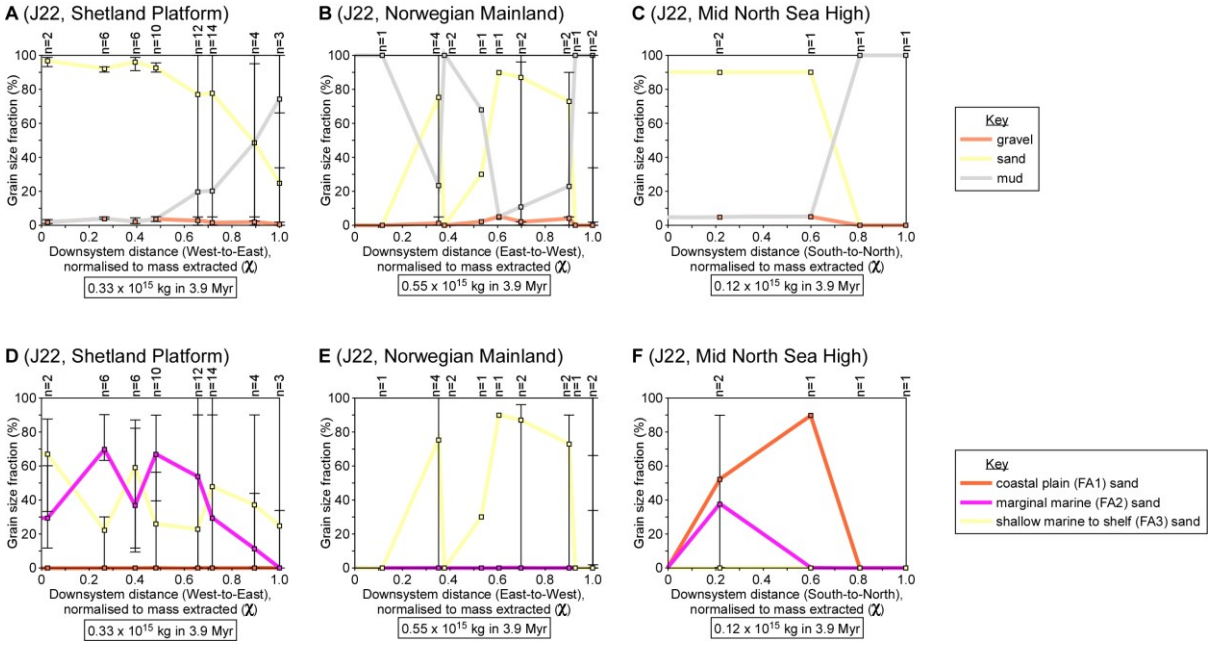


**Figure 10.** Downsystem variations in (**A-C**) percentage-thickness of gravel, sandstone and mudstone, and (**D-F**) percentage-thickness of coastal-plain, marginal-marine and shallow-marine sandstones for genetic sequence J22 (cf. Figs. 5, S2A-C) in the study well database (Fig. 4), as a function of sediment mass extracted ($\chi$) (Equation 1, Fig. 1). Downsystem variations are shown for: (**A, D**) transverse transect for western basin margin, sourced from Shetland Platform; (**B, E**) transverse transect for eastern basin margin, sourced from Norwegian Landmass; and (**C, F**) axial transect for southern basin margin, sourced from Mid-North Sea High (Fig. 5). Each point in the plots represents the mean value for a group of wells located at a specific downsystem distance, with the number of wells in the group indicated at the top of the plot (e.g. "n=3"). The vertical error bar for each point shows the variation in percentage-thickness values between wells in the group.

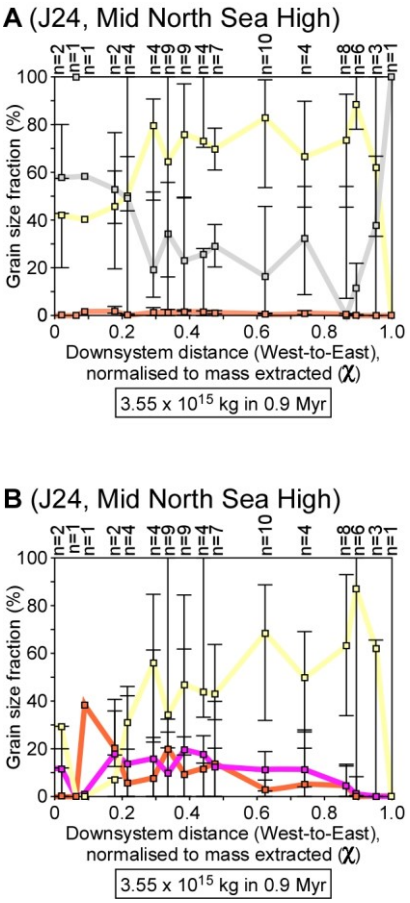


**Figure 11.** Downsystem variations in (**A**) percentage-thickness of gravel, sandstone and mudstone, and (**B**) percentage-thickness of coastal-plain, marginal-marine and shallow-marine sandstones for genetic sequence J24 (cf. Figs. 6, S2C) in the study well database (Fig. 4), as a function of sediment mass extracted ($\chi$) (Equation 1, Fig. 1). Downsystem variations are shown for axial transect along basin centre, sourced from Shetland Platform, Norwegian Landmass and Mid-North Sea High (Fig. 6). Each point in the plots represents the mean value for a group of wells located at a specific downsystem distance, with the number of wells in the group indicated at the top of the plot (e.g. "n=3"). The vertical error bar for each point shows the variation in percentage-thickness values between wells in the group. Key as for Figure 10.

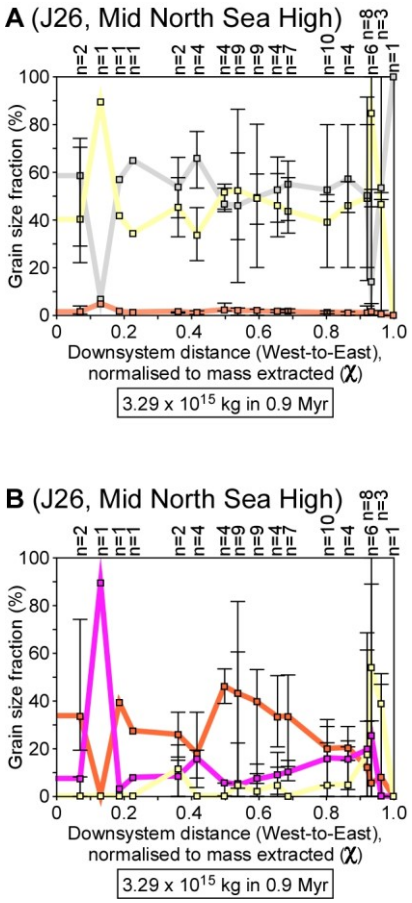


**Figure 12.** Downsystem variations in (A) percentage-thickness of gravel, sandstone and mudstone, and (B) percentage-thickness of coastal-plain, marginal-marine and shallow-marine sandstones for genetic sequence J26 (cf. Figs. 7, S2C) in the study well database (Fig. 4), as a function of sediment mass extracted ($\chi$) (Equation 1, Fig. 1). Downsystem variations are shown for axial transect along basin centre, sourced from Shetland Platform, Norwegian Landmass and Mid-North Sea High (Fig. 7). Each point in the plots represents the mean value for a group of wells located at a specific downsystem distance, with the number of wells in the group indicated at the top of the plot (e.g. "n=3"). The vertical error bar for each point shows the variation in percentage-thickness values between wells in the group. Key as for Figure 10.

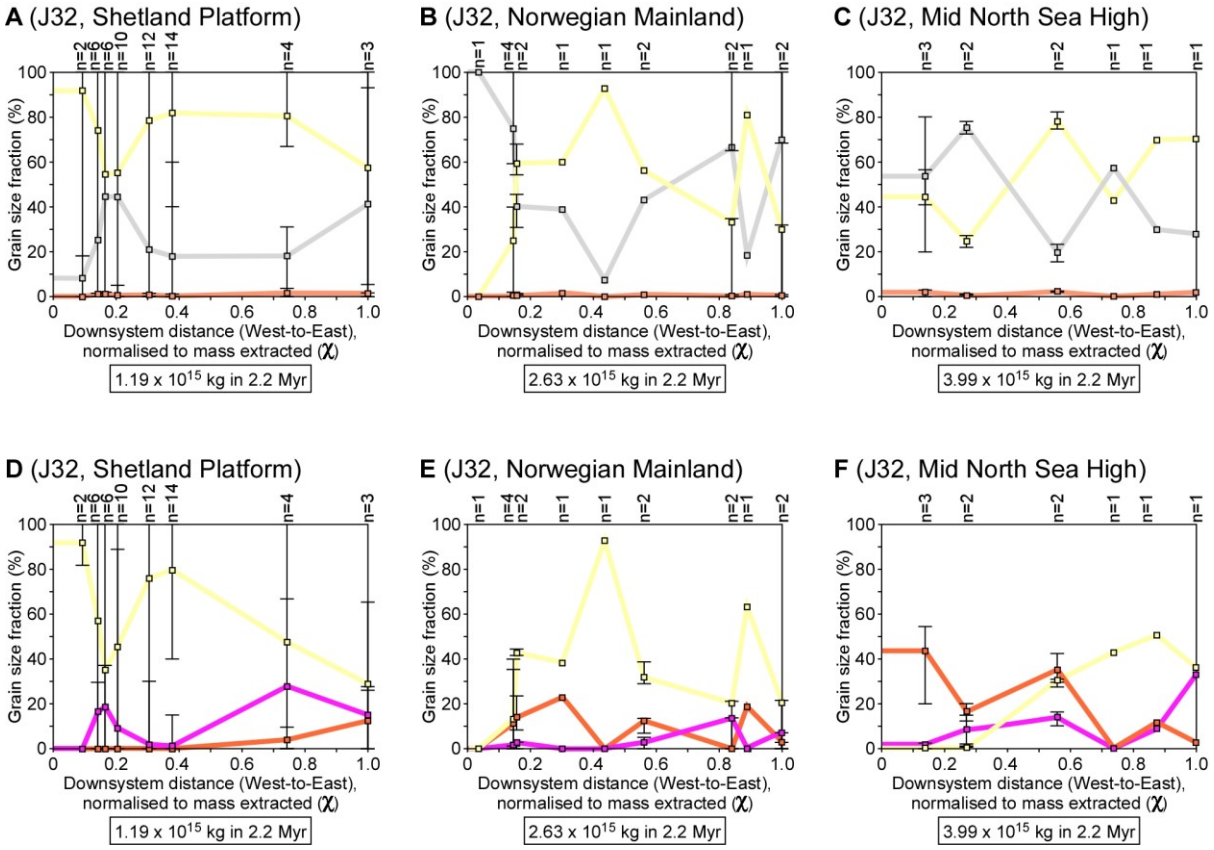


**Figure 13.** Downsystem variations in (**A-C**) percentage-thickness of gravel, sandstone and mudstone, and (**D-F**) percentage-thickness of coastal-plain, marginal-marine and shallow-marine sandstones for genetic sequence J32 (cf. Figs. 8, S2A-C) in the study well database (Fig. 4), as a function of sediment mass extracted ($\chi$) (Equation 1, Fig. 1). Downsystem variations are shown for: (**A, D**) transverse transect for western basin margin, sourced from Shetland Platform; (**B, E**) transverse transect for eastern basin margin, sourced from Norwegian Landmass; and (**C, F**) axial transect for southern basin margin, sourced from Mid-North Sea High (Fig. 8). Each point in the plots represents the mean value for a group of wells located at a specific downsystem distance, with the number of wells in the group indicated at the top of the plot (e.g. "n=3"). The vertical error bar for each point shows the variation in percentage-thickness values between wells in the group. Key as for Figure 10.

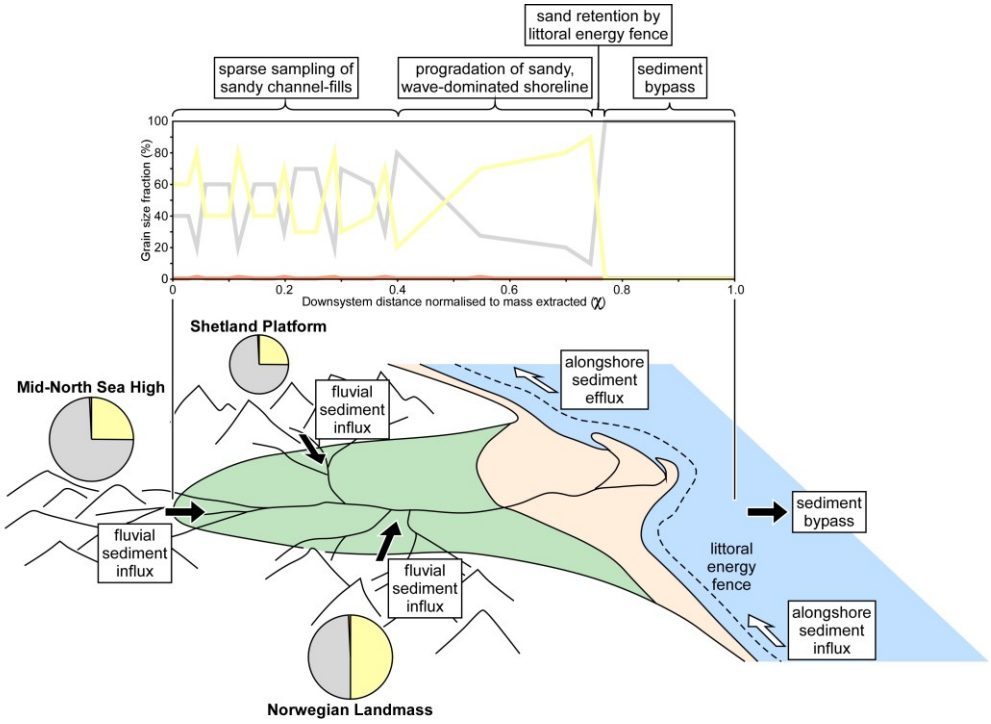


**Figure 14.** Conceptual model synthesising sediment source regions, sediment influxes and effluxes, depositional environments, and downsystem variations in gravel (orange), sandstone (yellow) and mudstone (grey) in the axial 'Brent Delta' sediment routing system. See text for discussion.

**Supplementary Material**

# DOWNSYSTEM GRAIN-SIZE TRENDS AND MASS BALANCE OF AN ANCIENT WAVE-INFLUENCED SEDIMENT ROUTING SYSTEM: MIDDLE JURASSIC BRENT DELTA, NORTHERN NORTH SEA, OFFSHORE UK AND NORWAY

IKENNA C. OKWARA[1,2], GARY J. HAMPSON*[1], ALEXANDER C. WHITTAKER[1] & GARETH G. ROBERTS[1]

[1]Department of Earth Science and Engineering, Imperial College London, South Kensington Campus, London SW7 2AZ, U.K.

[2] Department of Geology, University of Nigeria, Nsukka, Nigeria

*Corresponding author email address: g.j.hampson@imperial.ac.uk

**Table S1.** Wells in the study dataset (located in Fig. 4B), and previously published sequence stratigraphic frameworks (Fig. 3) that include interpretations of these wells.

| Well (Fig. 4B) | Well name | Stratigraphic interpretation (Fig. 3) |
|---|---|---|
| **1** | 34/2-4 | after Fjellanger et al. (1996) |
| **2** | 34/4-5 | after Mitchener et al. (1992) |
| **3** | 34/4-3 | after Sneider et al. (1995) |
| **4** | 211/13-6 | Penguin Field; after Mitchener et al. (1992), Fjellanger et al. (1996) |
| **5** | 211/19-6 | Murchison Field; after Hampson et al. (2004) |
| **6** | 211/18-21 | Don Field; after Mitchener et al. (1992) |
| **7** | 211/18-22 | Don Field; after Fjellanger et al. (1996) |
| **8** | 33/9-14 | Statfjord Nord Field; after Fjellanger et al. (1996) |
| **9** | 211/19-3 | Murchison Field; after Hampson et al. (2004) |
| **10** | 211/19-5 | after Hampson et al. (2004) |
| **11** | 211/19-1 | Thistle Field; after Hampson et al. (2004) |
| **12** | 211/18-19 | Thistle Field; after Hampson et al. (2004) |
| **13** | 211/16-6 | Eider Field; after Fjellanger et al. (1996), Hampson et al. (2004) |
| **14** | 210/20-2 | after Hampson et al. (2004) |
| **15** | 210/20-1 | after Hampson et al. (2004) |
| **16** | 210/25-2 | Tern Field; after Hampson et al. (2004) |
| **17** | 211/21-5 | Cormorant North Field; after Hampson et al. (2004) |
| **18** | 211/21-6 | Cormorant North Field; after Hampson et al., 2004) |
| **19** | 211/22-1 | after Hampson et al. (2004) |
| **20** | 211/22-2 | after Fjellanger et al. (1996) |
| **21** | 211/23-6 | Dunlin South West; after Mitchener et al. (1992) |
| **22** | 211/23-2 | Dunlin South West; after Hampson et al. (2004) |
| **23** | 211/24-5 | after Hampson et al. (2004) |
| **24** | 211/24-4 | Statfjord Field; after Fjellanger et al. (1996) |
| **25** | 33/9-3 | Statfjord Field; after Fjellanger et al. (1996) |
| **26** | 34/10-5 | Gullfaks Field; after Mitchener et al. (1992) |
| **27** | 34/8-1 | Visund Field; after Fjellanger et al. (1996) |
| **28** | 35/8-1 | Vega Field; after Fjellanger et al. (1996) |
| **29** | 35/8-3 | after Fjellanger et al. (1996) |
| **30** | 35/8-2 | Vega Field; after Sneider et al. (1995) |
| **31** | 35/11-2 | after Sneider et al. (1995) |
| **32** | 210/24-5 | after Hampson et al. (2004) |
| **33** | 211/26-2 | Cormorant South Field; after Hampson et al. (2004) |
| **34** | 211/27-3 | North West Hutton Field; after Mitchener et al. (1992) |
| **35** | 211/27-10 | North West Hutton Field; after Hampson et al. (2004) |
| **36** | 211/28-1 | Hutton Field; after Fjellanger et al. (1996), Hampson et al. (2004) |
| **37** | 211/28-5 | after Fjellanger et al. (1996), Hampson et al. (2004) |
| **38** | 211/29-3 | Brent Field; after Fjellanger et al. (1996), Hampson et al. (2004) |
| **39** | 211/29-2 | Brent Field; after Hampson et al. (2004) |
| **40** | 34/10-17 | Gullfaks Sør Field; after Fjellanger et al. (1996) |
| **41** | 34/10-23 | Valemon Field; after Fjellanger et al. (1996) |
| **42** | 2/5-3 | Heather Field; after Hampson et al. (2004) |
| **43** | 2/5-17 | Broom Field; after Hampson et al. (2004) |
| **44** | 3/1-1 | after Hampson et al. (2004) |
| **45** | 3/2-3 | Lyell Field; after Hampson et al. (2004) |

| | | |
|---|---|---|
| **46** | 3/2-4 | Lyell Field; after Hampson et al. (2004) |
| **47** | 3/2-6 | after Mitchener et al. (1992) |
| **48** | 3/3-3 | Ninian Field; after Mitchener et al. (1992), Hampson et al. (2004) |
| **49** | 3/3-7 | Ninian Field; after Hampson et al. (2004) |
| **50** | 3/3-8 | after Hampson et al. (2004) |
| **51** | 3/4-1 | Brent Field; after Hampson et al. (2004) |
| **52** | 3/4-13 | Strathspey Field; after Mitchener et al. (1992) |
| **53** | 3/4-9 | Strathspey Field; after Hampson et al. (2004) |
| **54** | 3/4-12 | Strathspey Field; after Hampson et al. (2004) |
| **55** | 3/4-8 | Alwyn North Field; after Hampson et al. (2004) |
| **56** | 30/2-2 | Huldra Field; after Fjellanger et al. (1996) |
| **57** | 31/2-4 | Troll Field; after Sneider et al. (1995) |
| **58** | 31/2-3 | Troll Field; after Sneider et al. (1995) |
| **59** | 2/10-2 | after Mitchener et al. (1992) |
| **60** | 3/7-5 | after Hampson et al. (2004) |
| **61** | 3/8-6 | Ninian Field; after Hampson et al. (2004) |
| **62** | 3/12-2 | after Mitchener et al. (1992) |
| **63** | 3/8-10 | Staffa Field; after Mitchener et al. (1992) |
| **64** | 3/8-1 | Ninian Field; after Mitchener et al. (1992) |
| **65** | 3/9-4 | Alwyn North Field; after Hampson et al. (2004) |
| **66** | 3/9-2 | Alwyn North Field; after Fjellanger et al. (1996) |
| **67** | 3/10-1 | after Hampson et al. (2004) |
| **68** | 29/6-1 | Martin Linge Field; after Fjellanger et al. (1996) |
| **69** | 30/9-2 | Oseberg Field; after Fjellanger et al. (1996) |
| **70** | 30/6-8 | after Fjellanger et al. (1996) |
| **71** | 31/4-3 | Brage Field; after Fjellanger et al. (1996) |
| **72** | 31/6-8 | Troll Field; after Fjellanger et al. (1996) |
| **73** | 30/9-8 | Oseberg Sør Field; after Fjellanger et al. (1996) |
| **74** | 30/11-3 | after Fjellanger et al. (1996) |
| **75** | 25/2-7 | after Fjellanger et al. (1996) |
| **76** | 79/9-3 | Bruce Field; after Mitchener et al. (1992) |
| **77** | 9/13-12 | Beryl Field; after Fjellanger et al. (1996) |
| **78** | 24/6-1 | after Fjellanger et al. (1996) |
| **79** | 15/3-3 | Gudrun Field; after Sneider et al. (1995), Kieft et al. (2011) |
| **80** | 15/3-1 | Gudrun Field; after Sneider et al. (1995), Kieft et al. (2011) |
| **81** | 15/3-4 | after Sneider et al. (1995), Kieft et al. (2011) |
| **82** | 15/9-3 | Sleipner Vest; after Sneider et al. (1995), Kieft et al. (2011) |
| **83** | 15/9-1 | Sleipner Vest; after Sneider et al. (1995), Kieft et al. (2011) |
| **84** | 15/9-2 | Sleipner Vest; after Sneider et al. (1995), Kieft et al. (2011) |
| **85** | 15/9-7 | Sleipner Vest; after Sneider et al. (1995), Kieft et al. (2011) |

**Table S2.** Cored intervals studied for selected wells (after table S1 of Okwara et al., 2023).

| Well | Field name | Top core (m/ft) | Base core (m/ft) | Core recovery | Thickness (m) | Core-wireline shift (m/ft) |
|---|---|---|---|---|---|---|
| 2/5-3 | Heather | 3350 m / 10992 ft | 346 m / 11362 ft | 100% | 113 | 3.0 m / 10 ft |
| 3/4a-12 | Strathspey | 2877 m / 9440 ft | 3141 m / 10306 ft | 100% | 264 | 1.8 m / 6 ft |
| 3/8b-10 | Staffa | 4052 m / 13294 ft | 4176 m / 13701 ft | 100% | 124 | 3.0 m / 10 ft |
| 9/9b-3 | Bruce | 3666 m / 12028 ft | 4002 m / 13130 ft | 88% | 296 | 1.5 m / 5 ft |
| 35/8-1 | Vega | 3523 m / 11557 ft | 3710 m / 12171 ft | 95% | 187 | 1.2 m / 4 ft |
| 210/20-2 | | 2858 m / 9375 ft | 2967 m / 9733 ft | 100% | 109 | 1.8 m / 6 ft |
| 211/19-6 | Murchison | 3205 m / 10516 ft | 3325 m / 10910 ft | 100% | 120 | 0.6 m / 2 ft |
| 30/2-2 | Huldra | 3939 m / 12923 ft | 4135 m / 13568 ft | 100% | 148 | 0 m / 0 ft |
| ***Total thickness*** | | | | | ***1361*** | |

**Table S3.** Calculated values of downsystem extraction of cumulative sediment mass normalised against the cumulative sediment mass in the sediment routing system volume ($\chi$; Equation 1) for genetic sequence J22 (Figs. 5, 10, S2).

| **transverse transect for western basin margin, sourced from Shetland Platform (Fig. 12A, D)** | | | |
|---|---|---|---|
| Wells at location | downsystem distance (km) | cumulative sediment mass extracted upsystem (x$10^{12}$ kg) | Proportion of total sediment mass extracted upsystem ($\chi$) |
| western boundary | 0 | 0 | 0 |
| 210/24a-5, 2/5-17 (n=2) | 16 | 8.70 | 0.03 |
| 2/5-3, 2/10a-2, 210/20-1, 210/20-2, 210/25-2, 211/26-2 (n=6) | 29 | 87.7 | 0.27 |
| 3/1-1, 3/2-3, 211/16-6, 211/21-5, 211/21-6, 211/22-1 (n=6) | 36 | 131 | 0.40 |
| 3/2-4, 3/2-6, 3/3-3, 3/7b-5, 3/8-6, 3/12-2, 211/22-2, 211/27-3, 211/27-10, 211/28-1 (n=10) | 44 | 159 | 0.48 |
| 3/3-8, 3/3-7, 3/8-1, 3/8b-10, 211/13-6, 211/18-19, 211/18a-21, 211/18-22, 211/19-1, 211/23-2, 211/23-6, 211/28-5 (n=12) | 57 | 217 | 0.66 |
| 3/4a-12, 3/4a-13, 3/4-1, 3/4-8, 3/4-9, 3/9-2, 3/9-4, 211/19-3, 211/19-5, 211/19-6, 211/24-2, 411/24-5, 211/29-2, 211/29-3 (n=14) | 62 | 237 | 0.72 |
| 33/9-3, 33/9-14, 29/6-1, 3/10-1 (n=4) | 77 | 295 | 0.89 |
| 34/10-5, 34/10-17, 34/4-3 (n=3) = eastern boundary | 87 | 330 | 1.00 |

| **transverse transect for eastern basin margin, sourced from Norwegian Landmass (Fig. 12B, E)** | | | |
|---|---|---|---|
| Wells at location | downsystem distance (km) | cumulative sediment mass extracted upsystem (x$10^{12}$ kg) | Proportion of total sediment mass extracted upsystem ($\chi$) |
| eastern boundary | 0 | 0 | 0 |
| 31/6-8 (n=1) | 39 | 64.2 | 0.12 |
| 31/2-3, 31/2-4, 35/8-3, 35/11-2 (n=4) | 58 | 194 | 0.35 |
| 35/8-1, 35/8-2 (n=2) | 60 | 208 | 0.38 |
| 31/4-3 (n=1) | 76 | 293 | 0.53 |
| 30/6-8 (n=1) | 85 | 334 | 0.61 |
| 30/9-2, 30/9-8 (n=2) | 91 | 385 | 0.70 |
| 30/2-2, 34/2-4 (n=2) | 107 | 496 | 0.90 |
| 34/8-1 (n=1) | 110 | 509 | 0.93 |
| 34/10-23, 34/4-5 (n=2) = eastern boundary | 119 | 550 | 1.00 |

| axial transect for southern basin margin, sourced from Mid-North Sea High (Fig. 12C, F) | | | |
|---|---|---|---|
| Wells at location | downsystem distance (km) | cumulative sediment mass extracted upsystem (x$10^{12}$ kg) | Proportion of total sediment mass extracted upsystem ($\chi$) |
| southern boundary | 0 | 0 | 0 |
| 24/6-1, 9/13-12st (n=2) | 50 | 26.4 | 0.22 |
| 9/9b-3 (n=1) | 74 | 72.2 | 0.60 |
| 25/2-7 (n=1) | 89 | 97.4 | 0.81 |
| 30/11-3 (n=1)<br>= northern boundary | 101 | 121 | 1.00 |

**Table S4.** Calculated values of downsystem extraction of cumulative sediment mass normalised against the cumulative sediment mass in the sediment routing system volume ($\chi$; Equation 1) for genetic sequence J24 (Figs. 6, 11, S2).

| **axial transect for southern basin margin, sourced from Shetland Platform, Norwegian Landmass and Mid-North Sea High (Fig. 13)** | | | |
|---|---|---|---|
| Wells at location | downsystem distance (km) | cumulative sediment mass extracted upsystem (x$10^{12}$ kg) | Proportion of total sediment mass extracted upsystem ($\chi$) |
| southern boundary | 0 | 0 | 0 |
| 24/6-1, 9/13-12st (n=2) | 109 | 81.5 | 0.02 |
| 25/2-7 (n=1) | 148 | 231 | 0.07 |
| 30/11-3 (n=1) | 160 | 323 | 0.09 |
| 30/9-2, 30/9-8 (n=2) | 197 | 639 | 0.18 |
| 29/6-1, 30/6-8, 31/4-3, 31/6-8 (n=4) | 211 | 773 | 0.22 |
| 2/10a-2, 3/8-6, 3/8b-10, 3/7b-5 (n=4) | 229 | 1050 | 0.30 |
| 3/2-6, 3/4-8, 3/8-1, 3/9-2, 3/9a-4, 3/10-1, 30/2-2, 31/2-3, 31/2-4 (n=9) | 237 | 1200 | 0.34 |
| 2/5-17, 3/1-1, 3/2-3, 3/2-4, 3/3-3, 3/3-7, 3/3-8, 3/4a-12, 3/4a-13 (n=9) | 246 | 1370 | 0.39 |
| 2/5-3, 3/4-1, 211/29-2, 34/10-23 (n=4) | 256 | 1580 | 0.44 |
| 211/26-2, 211/27-3, 211/27-10, 211/28-1, 211/28-5, 211/29-3, 34/10-17 (n=7) | 260 | 1690 | 0.48 |
| 210/24a-5, 211/21-5, 211/21-6, 211/22-2, 211/23-2, 211/23-6, 211/24-4, 211/24-5, 34/10-5, 35/11-2 (n=10) | 277 | 2220 | 0.63 |
| 210/25-2, 211/22-1, 33/9-3, 35/8-2 (n=4) | 289 | 2640 | 0.74 |
| 211/16-6, 211/18-19, 211/19-1, 211/19-3, 211/19-5, 34/8-1, 35/8-1, 35/8-2 (n=8) | 301 | 3080 | 0.87 |
| 210/20-1, 210/20-2, 211/18a-21, 211/18-22, 211/19-6, 33/9-14 (n=6) | 303 | 3180 | 0.90 |
| 211/13-6, 34/4-3, 34/4-5 (n=3) | 312 | 3390 | 0.96 |
| 34/2-4 (n=1) = northern boundary | 339 | 3550 | 1.00 |

**Table S5.** Calculated values of downsystem extraction of cumulative sediment mass normalised against the cumulative sediment mass in the sediment routing system volume ($\chi$; Equation 1) for genetic sequence J26 (Figs. 7, 12, S2).

| **axial transect for southern basin margin, sourced from Shetland Platform, Norwegian Landmass and Mid-North Sea High (Fig. 14)** | | | |
|---|---|---|---|
| Wells at location | downsystem distance (km) | cumulative sediment mass extracted upsystem (x$10^{12}$ kg) | Proportion of total sediment mass extracted upsystem ($\chi$) |
| southern boundary | 0 | 0 | 0 |
| 24/6-1, 9/13-12st (n=2) | 109 | 233 | 0.07 |
| 9/9b-3 (n=1) | 133 | 437 | 0.13 |
| 25/2-7 (n=1) | 148 | 617 | 0.19 |
| 30/11-3 (n=1) | 160 | 750 | 0.23 |
| 30/9-2, 30/9-8 (n=2) | 197 | 1190 | 0.36 |
| 29/6-1, 30/6-8, 31/4-3, 31/6-8 (n=4) | 211 | 1370 | 0.42 |
| 2/10a-2, 3/8-6, 3/8b-10, 3/7b-5 (n=4) | 229 | 1640 | 0.50 |
| 3/2-6, 3/4-8, 3/8-1, 3/9-2, 3/9a-4, 3/10-1, 30/2-2, 31/2-3, 31/2-4 (n=9) | 237 | 1770 | 0.54 |
| 2/5-17, 3/1-1, 3/2-3, 3/2-4, 3/3-3, 3/3-7, 3/3-8, 3/4a-12, 3/4a-13 (n=9) | 246 | 1960 | 0.60 |
| 2/5-3, 3/4-1, 211/29-2, 34/10-23 (n=4) | 256 | 2160 | 0.66 |
| 211/26-2, 211/27-3, 211/27-10, 211/28-1, 211/28-5, 211/29-3, 34/10-17 (n=7) | 260 | 2260 | 0.69 |
| 210/24a-5, 211/21-5, 211/21-6, 211/22-2, 211/23-2, 211/23-6, 211/24-4, 211/24-5, 34/10-5, 35/11-2 (n=10) | 277 | 2640 | 0.80 |
| 210/25-2, 211/22-1, 33/9-3, 35/8-2 (n=4) | 289 | 2850 | 0.87 |
| 211/16-6, 211/18-19, 211/19-1, 211/19-3, 211/19-5, 34/8-1, 35/8-1, 35/8-2 (n=8) | 301 | 3030 | 0.92 |
| 210/20-1, 210/20-2, 211/18a-21, 211/18-22, 211/19-6, 33/9-14 (n=6) | 303 | 3070 | 0.94 |
| 211/13-6, 34/4-3, 34/4-5 (n=3) | 312 | 3170 | 0.96 |
| 34/2-4 (n=1) = northern boundary | 339 | 3290 | 1.00 |

**Table S6.** Calculated values of downsystem extraction of cumulative sediment mass normalised against the cumulative sediment mass in the sediment routing system volume (χ) ; Equation 1 for genetic sequence J32 (Figs. 8, 13, S2).

| **transverse transect for western basin margin, sourced from Shetland Platform (Fig. 15A, D)** | | | |
|---|---|---|---|
| Wells at location | downsystem distance (km) | cumulative sediment mass extracted upsystem (x$10^{12}$ kg) | Proportion of total sediment mass extracted upsystem (χ) |
| western boundary | 0 | 0 | 0 |
| 210/24a-5, 2/5-17 (n=2) | 16 | 110 | 0.09 |
| 2/5-3, 2/10a-2, 210/20-1, 210/20-2, 210/25-2, 211/26-2 (n=6) | 29 | 168 | 0.14 |
| 3/1-1, 3/2-3, 211/16-6, 211/21-5, 211/21-6, 211/22-1 (n=6) | 36 | 196 | 0.17 |
| 3/2-4, 3/2-6, 3/3-3, 3/7b-5, 3/8-6, 3/12-2, 211/22-2, 211/27-3, 211/27-10, 211/28-1 (n=10) | 44 | 241 | 0.20 |
| 3/3-8, 3/3-7, 3/8-1, 3/8b-10, 211/13-6, 211/18-19, 211/18a-21, 211/18-22, 211/19-1, 211/23-2, 211/23-6, 211/28-5 (n=12) | 57 | 361 | 0.31 |
| 3/4a-12, 3/4a-13, 3/4-1, 3/4-8, 3/4-9, 3/9-2, 3/9-4, 211/19-3, 211/19-5, 211/19-6, 211/24-2, 411/24-5, 211/29-2, 211/29-3 (n=14) | 62 | 448 | 0.38 |
| 33/9-3, 33/9-14, 29/6-1, 3/10-1 (n=4) | 77 | 881 | 0.74 |
| 34/10-5, 34/10-17, 34/4-3 (n=3) = eastern boundary | 87 | 1190 | 1.00 |

| **transverse transect for eastern basin margin, sourced from Norwegian Landmass (Fig. 15B, E)** | | | |
|---|---|---|---|
| Wells at location | downsystem distance (km) | cumulative sediment mass extracted upsystem (x$10^{12}$ kg) | Proportion of total sediment mass extracted upsystem (χ) |
| eastern boundary | 0 | 0 | 0 |
| 31/6-8 (n=1) | 39 | 98.3 | 0.04 |
| 31/2-3, 31/2-4, 35/8-3, 35/11-2 (n=4) | 58 | 384 | 0.15 |
| 35/8-1, 35/8-2 (n=2) | 60 | 414 | 0.16 |
| 31/4-3 (n=1) | 76 | 794 | 0.30 |
| 30/6-8 (n=1) | 85 | 1150 | 0.44 |
| 30/9-2, 30/9-8 (n=2) | 91 | 1480 | 0.56 |
| 30/2-2, 34/2-4 (n=2) | 107 | 2210 | 0.84 |
| 34/8-1 (n=1) | 110 | 2340 | 0.89 |
| 34/10-23, 34/4-5 (n=2) = eastern boundary | 119 | 2630 | 1.00 |

| axial transect for southern basin margin, sourced from Mid-North Sea High (Fig. 15C, F) | | | |
|---|---|---|---|
| Wells at location | downsystem distance (km) | cumulative sediment mass extracted upsystem (x$10^{12}$ kg) | Proportion of total sediment mass extracted upsystem ($\chi$) |
| southern boundary | 0 | 0 | 0 |
| 15/9-2, 15/9-3, 15/9-7 (n=3) | 81 | 559 | 0.14 |
| 15/3-1, 15/3-3 (n=2) | 130 | 1090 | 0.27 |
| 24/6-1, 9/13-12st (n=2) | 198 | 2240 | 0.56 |
| 9/9b-3 (n=1) | 222 | 2950 | 0.74 |
| 25/2-7 (n=1) | 237 | 3490 | 0.88 |
| 30/11-3 (n=1)<br>= northern boundary | 249 | 3990 | 1.00 |

A

B

C

Depth (ft)
Seq. strat.
Lithostrat.
Facies ass.
Grain size and sedimentary structures
mud
sand
gravel
Sorting
Bio. index
Gamma ray
0 API 150
Density
1.7 g/cm³ 2.7
Neutron
60 p.u. 0
Sonic
140 us/ft 40
Resistivity
0.2 ohm-m 2000
HEATHER
TARBERT
NESS
ETIVE
RANNOCH
BROOM
OSEBERG
DRAKE
J32
J26
J24
J22
J32 (pars.)
HEATH.

**Sedimentary structures**

- High angle cross bed
- Low angle cross bed
- Wave ripple lamination
- Current ripple lamination
- Planar/flat lamination
- Bioturbation
- Mud drapes
- Mud or granule clasts
- Carbonaceous fragments
- Rootlets
- Soft sediment deformation
- Pyrite nodule
- Shell fragments
- Siderite nodule
- Stylolite

**1. Coastal plain FAs**

- 1.1. fluvial channel
- 1.2. floodplain
- 1.3. swamp

**2. Marginal marine FAs**

- 2.1. lagoon
- 2.2. fluvio-tidal / estuarine channel and fan delta
- 2.3. bay-head and lagoonal delta

**3. Shallow marine to shelf FAs**

- 3.1. weakly wave-influenced (bioturbated) shoreface
- 3.2. wave-dominated upper shoreface and barrier bar
- 3.3. proximal lower shoreface
- 3.4. distal lower shoreface and offshore

**Figure S1.** Sedimentological core logs and wireline logs of selected, representative wells from the Brent Delta routing system(s): (**A**) well 3/4a-12, Strathspey Field, offshore UK; (**B**) well 30/2-2, Huldra Field, offshore Norway; and (**C**) well 2/5-3, Heather Field, offshore UK (Table 2, Fig. 4; after Supplementary Material of Okwara et al., 2023). Core-defined facies associations (Table 1) are calibrated to wireline logs. Orange and grey colours in neutron-density log track indicate 'sand cross over' and 'shale cross over', respectively. Sequence stratigraphic divisions are synthesised from published literature (Fig. 3).

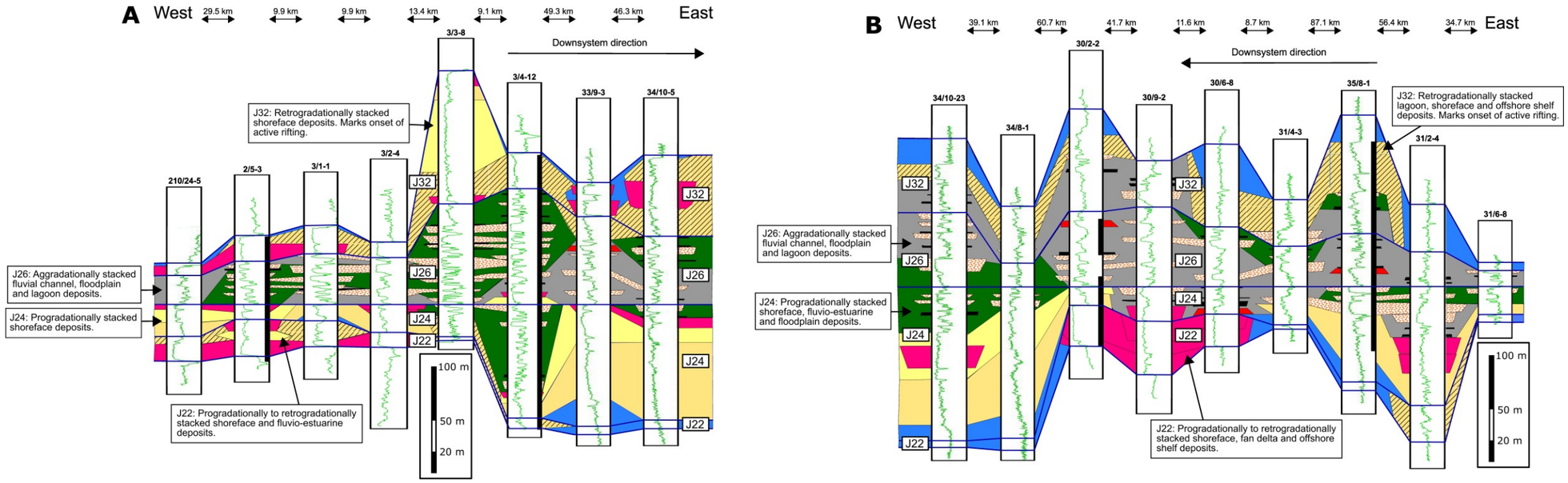
A West
29.5 km
9.9 km
9.9 km
13.4 km
9.1 km
49.3 km
46.3 km
East
Downsystem direction
3/3-8
3/4-12
33/9-3
34/10-5
210/24-5
2/5-3
3/1-1
3/2-4
J32: Retrogradationally stacked shoreface deposits. Marks onset of active rifting.
J26: Aggradationally stacked fluvial channel, floodplain and lagoon deposits.
J24: Progradationally stacked shoreface deposits.
J22: Progradationally to retrogradationally stacked shoreface and fluvio-estuarine deposits.
J32
J26
J24
J22
100 m
50 m
20 m
B West
39.1 km
60.7 km
41.7 km
11.6 km
8.7 km
87.1 km
56.4 km
34.7 km
East
Downsystem direction
34/10-23
34/8-1
30/2-2
30/9-2
30/6-8
31/4-3
35/8-1
31/2-4
31/6-8
J32: Retrogradationally stacked lagoon, shoreface and offshore shelf deposits. Marks onset of active rifting.
J26: Aggradationally stacked fluvial channel, floodplain and lagoon deposits.
J24: Progradationally stacked shoreface, fluvio-estuarine and floodplain deposits.
J22: Progradationally to retrogradationally stacked shoreface, fan delta and offshore shelf deposits.
J32
J26
J24
J22
100 m
50 m
20 m
C South
50.2 km
81.1 km
24.2 km
56.5 km
16.5 km
49.3 km
46.3 km
37.9 km
16.3 km
11.0 km
11.5 km
9.0 km
16.8 km
20.8 km
14.8 km
15.7 km
10.3 km
22.9 km
32.6 km
North
15/9-2
15/3-3
24/6-1
9/9-3
25/2-7
30/11-3
3/8-10
3/9-4
3/4-12
211/28-5
211/24-4
33/9-3
211/19-3
33/9-14
34/4-3
34/2-4
30/9-2
29/6-1
3/12-2
3/4-1
1. Coastal plain FAs
1.1. fluvial channel
1.2. floodplain
1.3. swamp
2. Marginal marine FAs
2.1. lagoon
2.2. fluvio-tidal / estuarine channel and fan delta
2.3. bay-head and lagoonal delta
3. Shallow marine to shelf FAs
3.1. weakly wave-influenced (bioturbaed) shoreface
3.2. wave-dominated upper shoreface and barrier bar
3.3. proximal lower shoreface
3.4. distal lower shoreface and offshore
Downsystem direction
Onlap on Triassic? basement during J32 transgression
J32: Retrogradationally stacked shoreface deposits. Marks onset of active rifting.
J26: Aggradationally stacked fluvial channel and floodplain deposits.
J22: Progradationally to retrogradationally stacked shoreface and fluvio-estuarine deposits.
J24: Progradationally stacked shoreface deposits.
Rapid northward thinning of all units towards downsystem termination?
Fault terrace with expressed inherited topography?
Sleipner Formation
Bruce - Upper Sands
Bruce - A
Bruce - B
Bruce - C
Tarbert
Ness Formation
Etive
Rannoch
Broom
J32
J26
J24
J22
100 m
50 m
20 m

**Figure S2.** Regional sequence stratigraphic correlation panels: (**A**) transverse panel from the western basin margin, adjacent to the Shetland Platform source area, to the basin centre; (**B**) transverse panel from the eastern basin margin, adjacent to the Norwegian Landmass source area, to the basin centre; and (**C**) axial panel from the southern basin margin, adjacent to the Mid North Sea High source area, to the northern limit of the basin (after Mitchener et al., 1992; Sneider et al., 1995; Fjellanger et al., 1996; Hampson et al., 2004; figure 5 of Okwara et al., 2023). Panels are located in Figure 4, and flattened on the top of the J24 genetic sequence. Given the large well spacing, only stratigraphic surfaces bounding genetic sequences J22, J24, J26 and J32 (Fig. 3) are shown.